shown that ADCC is an important anti-tumor mechanism utilized in vivo against Her2/neu+ tumor cells [13,14]. ADCC conducted by NK cells in vitro is enhanced by IL-2 activation and is critically dependent on interactions between FcγRIII on NK cells and Trastuzumab-coated tumor targets [15]. Clynes et al. have shown that the anti-tumor effects of Trastuzumab in a murine model of breast cancer require the expression of functional Fc receptors by immune effectors [16]. Blockade of FCγRIII with anti-CD16 mAb inhibited ADCC by approximately 80% compared to NK cells incubated with control IgG [15]. Recently, our studies reported that involvement of NK cells is critical for tumor growth and metastasis of cancer and virus-infected cells in murine model [17,18] and autologous activated NK cells could be useful for cancer and viral immunotherapy [19]. However, role of natural killer activities in the course of cancer progression in human remains one of the major issues in tumor immunology and immunotherapy.

In the present study, we investigated the natural killer activities of breast cancer patients. We found that natural killer activities of peripheral-blood mononuclear cells (PBMCs) from breast cancer patients were substantially lower than from healthy individuals. HER2-negative breast cancer patients had lower natural killer activity as compared with HER2-positive patients. Thus, our results suggest that natural killer activity of immune cells might play a critical role to progression of cancer in patients.

2. Materials and methods

2.1. Collection of human specimens and isolation of PBMCs

The Ethical Review Committee of the Institute approved the experimental protocol. Blood was collected after obtaining informed consent from breast cancer patients and healthy volunteers. PBMCs were isolated from the blood by Ficoll-Hypaque gradient centrifugation (Amersham Biosciences, Uppsala, Sweden) and washed twice with RPMI1640 and counted the number of cells by trypan blue.

2.2. Culture of cell line

Erythroleukemia cell line K562 was cultured in RPMI1640 medium supplemented with 10% heat-inactivated fetal bovine serum (JRH Biosciences, Lenexa, KS), 100 U/ml penicillin, and 10 μg/ml streptomycin.

2.3. Cytotoxic activity

Freshly isolated PBMCs and activated NK cells were tested for cytotoxic activity at various effector-to-target (E/T) ratios in a Calcein-AM release assay using TERASCAN VP (Minerva Tech., Tokyo, Japan). We labeled the target cells K562 with immunofluorescent-dye Calcein-AM solution (Do Jindo Lab., Kumamoto, Japan) and incubated for 30 min and followed by washing the cells with PBS(−) and checked the fluorescence intensity of cells. Target cells and effector cells were suspended with RPMI1640 and 10% fetal bovine serum at various E/T ratios and added into 96-well plate and followed by incubation for 2 h and again checked the fluorescence intensity.

2.4. Statistical analysis

The statistical analysis was performed using StatView for Windows, Version 5.0.

3. Results and discussion

Totally 89 individuals were enrolled in this study and agreed to give peripheral-blood samples. Among them 71 were breast cancer patients (61 primary and 10 metastatic patients) and 18 healthy volunteers. Baseline characteristics for primary cancer patients who entered the study are shown in Table 1. Average age of healthy donors is 30 (20–70) years, used in this study as control, average age of primary breast cancer patients is 55 (31–84) years and average age of metastatic cancer patients is 59 (36–69) years.

Table 1
Clinico-pathological data of the primary breast cancer patients.

	$n=61$
Age	
Median (min–max)	55 (31–84)
Menopause	
Pre	21 (34.4%)
Post	40 (65.6%)
Histological type	
Ductal carcinoma in situ	7 (11.5%)
Invasive ductal carcinoma	50 (82.0%)
Others	3 (4.9%)
Unknown	1 (1.6%)
Tumor size	
T1	17 (27.9%)
T2	37 (60.7%)
T3	6 (9.8%)
T4	1 (1.6%)
Lymph node	
N0	41 (67.3%)
N1	18 (29.5%)
N2	1 (1.6%)
Unknown	1 (1.6%)
Estrogen receptor	
Positive	37 (60.6%)
Negative	14 (23.0%)
Unknown	10 (16.4%)
Progesterone receptor	
Positive	27 (44.3%)
Negative	24 (39.3%)
Unknown	10 (16.4%)
HER2 (IHC[a])	
0	14 (23.0%)
1+	22 (36.1%)
2+	6(9.8%)
3+	8 (13.1%)
Unknown	11 (18.0%)

[a] Immunohistochemical (HercepTest™).

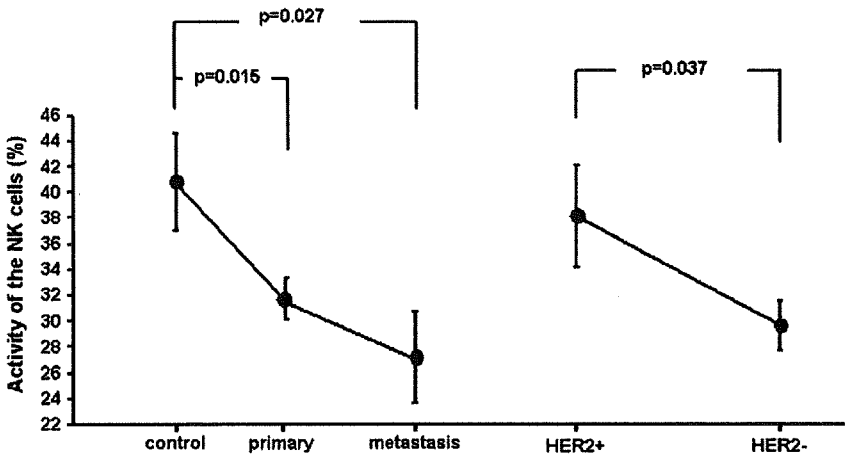

Fig. 1. NK activity in cancer patients. Spontaneous cytotoxic activity of freshly isolated PBMCs from breast cancer patients was done against K562 cells at different E/T ratios. Averages were calculated on healthy donors versus various cancer patients with statistical analysis. Natural killer activity of breast cancer patients with primary and metastatic tumor was compared with healthy donors and natural killer activity of breast cancer patients with HER2-positive (IHC 2+ and 3+) and -negative (IHC 0 and 1+). The number of healthy donors 18 and number of patients such as primary 61, metastasis 10, HER2-positive 14 and -negative 36 were enrolled in this study.

In patients with cancer and viral infection, NK-cell function has been shown to be impaired [20,21]. To check the natural killer activity, we examined the natural cytotoxic activity of freshly isolated PBMCs from patients with breast cancer and healthy individuals against susceptible K562 erythroleukemia cell line. Natural killer activity of PBMCs was significantly lower in patients with breast cancer than that of healthy individuals (Fig. 1 and Table 2). Furthermore, the ability to kill K562 target cells was clearly reduced in PBMCs from HER2-negative 36 cancer patients than 14 patients with HER2-positive tumors (Fig. 1). No statistical association was found between the natural killer activities and primary and metastatic tumor, tumor sizes, age groups and hormone receptors (data not shown). Total number of T cells and lymphocytes were substantially lower in breast cancer patients as compared with healthy donors (Table 2). There were no statistical differences among the two groups of study subjects in the median number of NK cells and its subsets and WBC (Table 2). These results suggest that natural killer activities are important for breast cancer development and disease progression.

Table 2
Immunological status of the patients and healthy donors.

	Patients	Healthy donors	*p*-value (*t*-test)
Natural killer activity (%)	31.1	40.8	0.007
Number of the NK cells (/microL)	137.5	167.1	N.S.
Number of the CD16+/CD56 − cells (/microL)	34.1	35.6	N.S.
Number of the CD16+/CD56 + cells (/microL)	134.9	155.2	N.S.
Number of the CD4+/CD25 + cells (/microL)	74.5	32.5	N.S.
Number of the T cells (/microL)	724.7	959.5	0.004
Number of the lymphocyte (/microL)	1064.9	1438.5	0.002
Number of the WBC (/microL)	4644.2	5176.9	N.S.

In summary, our results suggest that NK activity of immune cells may play a critical role in tumor growth and metastasis, and that autologous activated NK cells could be a promising immunotherapeutic strategy against cancer either alone or in combination with humanized anti-tumor antibodies as a logical approach to the immunotherapy of cancer.

Conflict of interest

The authors have declared that no conflict of interest exists.

Acknowledgements

This work was supported by grants from the Ministry of Education, Science and Culture; the Ministry of Health, Labor and Welfare; and Human Health Science of Japan.

References

[1] Nicolson GL. Paracrine and autocrine growth mechanisms in tumor metastasis to specific sites with particular emphasis on brain and lung metastasis. Cancer Metastasis Rev 1993;12:325–43.
[2] Kim H, Muller WJ. The role of the epidermal growth factor receptor family in mammary tumorigenesis and metastasis. Exp Cell Res 1999; 253:78–87.
[3] Hyder SM, Chiappetta C, Stancel GM. Pharmacological and endogenous progestins induce vascular endothelial growth factor expression in human breast cancer cells. Int J Cancer 2001;92:469–73.
[4] McEarchern JA, Kobie JJ, Mack V, Wu RS, Meade-Tollin L, Arteaga CL, et al. Invasion and metastasis of a mammary tumor involves TGF-beta signaling. Int J Cancer 2001;91:76–82.
[5] Muller A, Homey B, Soto H, Ge N, Catron D, Buchanan ME, et al. Involvement of chemokine receptors in breast cancer metastasis. Nature 2001;410:50–6.
[6] Trinchieri G. Biology of natural killer cells. Adv Immunol 1989;47:187–376.
[7] Imai K, Matsuyama S, Miyake S, Suga K, Nakachi K. Natural cytotoxic activity of peripheral-blood lymphocytes and cancer incidence: an 11-year follow-up study of a general population. Lancet 2000;356:1795–9.

[8] Ullum H, Gotzsche PC, Victor J, Dickmeiss E, Skinhøj P, Pedersen BK. Defective natural immunity: an early manifestation of human immunodeficiency virus infection. J Exp Med 1995;182:789–99.
[9] Ahmad R, Menezes J. Defective killing activity against gp120/41-expressing human erythroleukaemic K562 cell line by monocytes and natural killer cells from HIV-infected individuals. AIDS 1996;10:143–9.
[10] Scott-Algara D, Paul P. NK cells and HIV infection: lessons from other viruses. Curr Mol Med 2002;2:757–68.
[11] Bonaparte MI, Barker E. Inability of natural killer cells to destroy autologous HIV-infected T lymphocytes. AIDS 2003;17:487–94.
[12] Carter P, Presta L, Gorman CM, Ridgway JB, Henner D, Wong WL, et al. Humanization of an anti-p185HER2 antibody for human cancer therapy. Proc Natl Acad Sci U S A 1992;89:4285–9.
[13] Tokuda Y, Ohnishi Y, Shimamura K, Iwasawa M, Yoshimura M, Ueyama Y, et al. In vitro and in vivo anti-tumour effects of a humanised monoclonal antibody against c-erbB-2 product. Br J Cancer 1996;73:1362–5.
[14] Sliwkowski MX, Lofgren JA, Lewis GD, Hotaling TE, Fendly BM, Fox JA. Nonclinical studies addressing the mechanism of action of trastuzumab (Herceptin). Semin Oncol 1999;26:60–70.
[15] Carson WE, Parihar R, Lindemann MJ, Personeni N, Dierksheide J, Meropol NJ, et al. Interleukin-2 enhances the natural killer cell response to Herceptin-coated Her2/neu-positive breast cancer cells. Eur J Immunol 2001;31:3016–25.
[16] Clynes RA, Towers TL, Presta LG, Ravetch JV. Inhibitory Fc receptors modulate in vivo cytoxicity against tumor targets. Nat Med 2000;6:443–6.
[17] Dewan MZ, Terunuma H, Takada M, Tanaka Y, Abe H, Sata T, et al. Role of natural killer cells in hormone-independent rapid tumor formation and spontaneous metastasis of breast cancer cells in vivo. Breast Cancer Res Treat 2007;104:267–75.
[18] Dewan MZ, Terunuma H, Toi M, Tanaka Y, Katano H, Deng X, et al. Potential role of natural killer cells in controlling growth and infiltration of AIDS-associated primary effusion lymphoma cells. Cancer Sci 2006;97:1381–7.
[19] Terunuma H, Deng X, Dewan MZ, Fujimoto S, Yamamoto N. Potential role of NK cells in the induction of immune responses: implications for NK cell-based immunotherapy for cancers and viral infections. Int Rev Immunol 2008;27:93–110.
[20] Whiteside TL, Herberman RB. Role of human natural killer cells in health and disease. Clin Diagn Lab Immunol 1994;1:125–33.
[21] Whiteside TL, Vujanovic NL, Herberman RB. Natural killer cells and tumor therapy. Curr Top Microbiol Immunol 1998;230:221–44.

Int. J. Cancer: **124,** 622–629 (2009)

An HIV protease inhibitor, ritonavir targets the nuclear factor-kappaB and inhibits the tumor growth and infiltration of EBV-positive lymphoblastoid B cells

Md. Zahidunnabi Dewan[1,2], Mariko Tomita[3], Harutaka Katano[4], Norio Yamamoto[1], Sunjida Ahmed[1], Michiko Yamamoto[5], Tetsutaro Sata[4], Naoki Mori[3]* and Naoki Yamamoto[1,2]*

[1]*Department of Molecular Virology, Graduate School, Tokyo Medical and Dental University, 1-5-45 Yushima, Bunkyo-ku, Tokyo 113-8519, Japan*
[2]*AIDS Research Center, National Institute of Infectious Diseases, 1-23-1 Toyama, Shinjuku-ku, Tokyo 162-8640, Japan*
[3]*Division of Molecular Virology and Oncology, Graduate School of Medicine, University of the Ryukyus, 207 Uehara, Nishihara, Okinawa 903-0215, Japan*
[4]*Department of Pathology, National Institute of Infectious Diseases, 1-23-1 Toyama, Shinjyuku-ku, Tokyo 162-8640, Japan*
[5]*Division of Safety Information on Drug, National Institute of Health Sciences, Food and Chemicals, Setagaya-ku, Tokyo 158-8501, Japan*

Epstein-Barr Virus (EBV)-associated immunoblastic lymphoma occurs in immunocompromised patients such as those with AIDS or transplant recipients after primary EBV infection or reactivation of a preexisting latent EBV infection. In the present study, we evaluated the effect of ritonavir, an HIV protease inhibitor, on EBV-positive lymphoblastoid B cells *in vitro* and in mice model. We found that it induced cell-cycle arrest at G_1-phase and apoptosis through down-regulation of cell-cycle gene cyclin D2 and anti-apoptotic gene survivin. Furthermore, ritonavir suppressed transcriptional activation of NF-κB in these cells. Ritonavir efficiently prevented growth and infiltration of lymphoma cells in various organs of NOD/SCID/γc^{null} mice at the same dose used for treatment of patients with AIDS. Our results indicate that ritonavir targets NF-κB activated in tumor cells and shows anti-tumor effects. These data also suggest that this compound may have promise for treatment or prevention of EBV-associated lymphoproliferative diseases that occur in immunocompromised patients.

Key words: ritonavir; LCLs; NF-κB; NOG mice

Epstein-Barr virus (EBV) is a ubiquitous human γ herpes virus that establishes a latent infection more than 90% of adults worldwide.[1] Immunocompromised individuals such as those with AIDS or transplant recipients are at increased risk for developing aggressive EBV-associated lymphoproliferative diseases. EBV is associated with malignant diseases, including Burkitt's lymphoma,[1,2] nasopharyngeal carcinoma[3,4] and immunoblastic B cell lymphoma of immunosuppressed individuals. Infection of primary B cells with EBV results in transformation with growth of the cells in tight clumps and immortalization of the cells. These immortalized B cells have an immunoblastic morphology and express each of the EBV-encoded small RNAs (EBERs), EBV nuclear antigen (EBNAs) and latent membrane proteins (LMPs).[2,5] EBERs have oncogenic potential through inhibition of PKR.[6] EBNA-2 is a transactivator that up-regulates expression of cellular genes and LMPs. LMP-1 may mediate proliferative and survival effects not only in EBV-transformed B lymphocytes but also in these malignancies that occur long after primary infection. Many immunocompromised patients with EBV-associated immunoblastic lymphoma have tumors at extranodal sites such as the brain, lung, or gastrointestinal tract. The prognosis of EBV-associated lymphomas is very poor for patients with irreversible immunosuppression and treatment options are limited.

Despite the diversity in clinical manifestations of hematopoietic malignancies, strong and constitutive nuclear factor-kappaB (NF-κB) activation was reported to be a unique and common characteristic of malignant cells.[7,8] In resting cells, NF-κB is sequestered as an inactive precursor by association with inhibitory IκBs in the cytoplasm. On stimulation, IκBs are rapidly phosphorylated, ubiquitinated and degraded by a proteasome-dependent pathway allowing active NF-κB to translocate into the nucleus where it can activate the expression of a number of genes.[9] LMP-1 is an oncoprotein that constitutively activates NF-κB to induce B cell proliferation.[7] Lymphoblastoid cell lines (LCLs) express high level of the antiapoptotic proteins BCL-2, BCL-xL, c-IAP1, Bfl-1 and c-FLIP the targets of NF-κB.[10,11] NF-κB activation has been connected with multiple processes of oncogenesis including control of apoptosis, cell-cycle, differentiation and cell migration,[9] and therefore, inhibition of NF-κB was suggested to be a useful strategy for cancer therapy.[12–20] It has been also reported that inhibition of NF-κB in EBV-associated lymphomas results in induction of apoptosis.[21] Therefore, targeting the NF-κB pathway and inhibition of NF-κB activity is a logical strategy for treating EBV-associated lymphomas.

Ritonavir, a human immunodeficiency virus type 1(HIV-1) protease inhibitor, has been successfully used in clinical treatments of HIV infection, with patients exhibiting a marked decrease in HIV viral load and a subsequent increase in $CD4^+$ T-cell counts.[22–25] Evidence of other effects by ritonavir on cellular proteases, such as the cysteine proteases cathepsin D and E, was presented in the drug's original description, albeit at concentrations >500-fold above the concentration required for inhibition of HIV protease.[26] Protease inhibitors have also been shown to directly affect cell metabolism, interfere with host or fungal proteases and block T-cell activation and dendritic-cell function.[27,28] Ritonavir has been shown to inhibit the chymotrypsin-like activity of the 20S proteasome, and it activates the chymotrypsin-like activity of the 26S proteasome conversely.[27,29,30] Ritonavir also has been reported to inhibit the transactivation of NF-κB induced by activators such as TNFα, HIV-1 Tat protein and the human herpesvirus 8 protein ORF74.[31] It is possible that inhibition of NF-κB activation by ritonavir is linked to additional pathways other than inhibition of proteasome.[31] Protease inhibitors also have been shown to have direct antiangiogenic and antitumor activity.[31,32] Recently, we reported that ritonavir inhibits growth and infiltration of ATL cells through targeting NF-κB.[20]

Grant sponsors: Ministry of Education, Science and Culture, The Ministry of Health, Labor and Welfare, Human Health Science of Japan.

Md. Zahidunnabi Dewan's current address is: Department of Pathology, New York University School of Medicine, 550 First Avenue, New York, NY 10016, USA.

Md. Zahidunnabi Dewan and Mariko Tomita contributed equally to this work.

***Correspondence to:** AIDS Research Center, National Institute of Infectious Diseases, 1-23-1 Toyama, Shinjuku-ku, Tokyo 162-8640, Japan. Fax: 8135-285-1165. E-mail: nyama@nih.go.jp (or) Division of Molecular Virology and Oncology, Graduate School of Medicine, University of the Ryukyus, 207 Uehara, Nishihara, Okinawa 903-0215, Japan.
Fax: 81-98-895-1410. E-mail: n-mori@med.u-ryukyu.ac.jp.

Received 14 July 2008; Accepted after revision 2 September 2008
DOI 10.1002/ijc.23993
Published online 15 September 2008 in Wiley InterScience (www.interscience.wiley.com).

UICC Publication of the International Union Against Cancer

In the present, we demonstrate that inhibition of NF-κB activity by ritonavir results in marked increase of apoptosis and induce cell-cycle arrest in EBV-positive lymphoblastoid B cells. We found that ritonavir also suppresses the expression of genes involved in antiapoptosis and cell-cycle progression. In addition, we established preclinical models using newly developed NOD/SCID/γc^{null} (NOG) mouse,[16] a unique type of animal, lacking T-, B- and NK-cells to evaluate the efficacy of antitumor and anti-NF-κB therapies. In the murine model, ritonavir at the clinically relevant dose potently inhibited the growth and infiltration of EBV-transformed LCL cells.

Material and methods

Mice and cells

NOG mice were obtained from the Central Institute for Experimental Animals (Kawasaki, Japan). All mice were maintained under specific-pathogen-free conditions in the Animal Center of Tokyo Medical and Dental University (Tokyo, Japan). The Ethical Review Committee of the Institute approved the experimental protocol.

EBV-positive immortalized lymphoblatoid B-cell lines (LCL-Ya, LCL-Ao, LCL-Ka and LCL-Ku) were cultured in RPMI 1640 medium supplemented with 10% heat-inactivated fetal bovine serum (JRH Biosciences, Lenexa, KS), 100 U/ml penicillin, and 10 μg/ml streptomycin. Peripheral blood mononuclear cells (PBMCs) from 3 healthy volunteers were analyzed. Mononuclear cells were isolated by Ficoll-Paque density gradient centrifugation (GE Healthcare Biosciences, Uppsala, Sweden) and washed with PBS.

Cell viability assay

The effect of ritonavir on cell viability of LCLs and PBMCs from healthy donors was examined by the reagent, water-soluble tetrazolium (WST)-8 (Wako Chemicals, Osaka, Japan). Briefly, 2×10^5 cells were incubated in a 96-well microculture plate in the absence or presence of various concentrations of ritonavir. After 72 hr of culture, WST-8 (5 μl) was added for the last 4 hr of incubation and absorbance at 450 nm was measured using an automated microplate reader. Measurement of mitochondrial dehydrogenase cleavage of WST-8 to formazan dye provides an indication of the level of cell viability.

Cell-cycle analysis

Cells were plated at a density of 3×10^5/ml in 60-mm tissue culture dishes. Twelve hours after plating, cells were exposed to 40 μM ritonavir for 24 h. Cell-cycle analysis was performed with the CycleTEST PLUS DNA reagent kit (Becton Dickinson, San Jose, CA). Briefly, cells were washed with a buffer solution containing sodium citrate, sucrose and dimethyl sulfoxide, suspended in a solution containing RNase A, and stained with 125 μg/ml propidium iodide (PI) for 10 min. Cell suspensions were analyzed on EPICS XL flow cytometer (Beckman Coulter, Fullerton, CA) using EXPO32 software. The cell population at each cell-cycle phase was determined with MultiCycle software (Beckman Coulter).

Assay for apoptosis

Cells were plated at a density of 3×10^5/ml in 60-mm tissue culture dishes. Twelve hours after plating, cells were exposed to ritonavir for 72 hr. Apoptosis was quantified by double staining with Annexin-V-Fluos (Roche Diagnostics, Mannheim, Germany) and PI (Backman Coulter) according to the instructions supplied by the manufacturer. Cells were analyzed on EPICS XL flow cytometer (Beckman Coulter) using EXPO32 software.

Western blot analysis

Treated cells were solubilized at 4°C in lysis buffer containing 62.5 mM Tris-HCl (pH 6.8), 2% SDS, 10% glycerol, 6% 2-mercaptoethanol and 0.01% bromophenol blue. Samples were subjected to electrophoresis on SDS-polyacrylamide gels followed by transfer to a polyvinylidine difluoride membrane and probing with the following specific antibodies: polyclonal antibodies against survivin, cyclin D2 (Santa Cruz Biotechnology, Santa Cruz, CA), Bcl-X_L (BD Transduction Laboratories, San Jose, CA) and monoclonal antibodies against Bcl-2, p53, actin (NeoMarkers, Fremont, CA), PARP (BD Transduction Laboratories) and LMP-1 (DAKO, Kyoto, Japan). The protein bands recognized by the antibodies were visualized using the enhanced chemiluminescence system (Amersham, Piscataway, NJ).

Electrophoresis mobility shift assay (EMSA)

Cells were placed in culture at 1×10^6 cells/ml and examined for inhibition of NF-κB 24 hr after exposure to ritonavir. Nuclear proteins were extracted, and NF-κB binding activities to κB element were examined by EMSA as described previously.[8] In brief, 5 μg of nuclear extracts were preincubated in a binding buffer containing 1 μg of poly (dI:dC) (Amersham Biosciences), followed by addition of ^{32}P-labeled oligonucleotide probe containing NF-κB element (5×10^4 c.p.m.). These mixtures were incubated for 15 min at room temperature. The DNA-protein complexes were separated on a 4% polyacrylamide gel and visualized by autoradiography. To examine the specificity of the NF-κB element probe, unlabeled competitor oligonucleotides were preincubated with nuclear extracts for 15 min before incubation with probes. The probe or competitors used were prepared by annealing the sense and antisense synthetic oligonucleotides as follows: a typical NF-κB element from the *IL-2Rα* gene, 5′-gatcCGGCAGGGGAATCTCCCTCTC-3′; and AP-1 element of the *IL-8* gene, 5′-gactGTGATGACTCAGGTT-3′. Underlined sequences represent the NF-κB or AP-1 binding site. To identify NF-κB protein in the DNA protein complex revealed by EMSA, we used antibodies specific for various NF-κB proteins, including p50, p65, c-Rel, RelB and p52 (Santa Cruz Biotechnology), to elicit a supershift DNA protein complex formation. These antibodies were incubated with the nuclear extracts for 45 min at room temperature before incubation with radiolabeled probes.

Inoculation of EBV-positive immortalized LCLs and collection of samples

LCL Cells [LCL-Ya, LCL-Ao, LCL-Ka and LCL-Ku] were washed twice with serum-free RPMI-1640 medium and resuspended in same medium. Mice were anaesthetized with ether and cells were inoculated subcutaneously (sc) in the postauricular region of NOG mice at a dose of 1×10^7 cells per mouse. All mice were sacrificed 3 weeks after inoculation with lymphoma cells. We measured tumor size 3 weeks after inoculation. Tissues and various organs of mice were collected and fixed with Streck Tissue Fixative, then processed to paraffin wax-embedded sections for staining with hematoxylin and eosin (HE) and immunostaining.

PCR primer and conditions

Detection of the BamHI W repeat region of the EBV genome was performed using 100 ng of genomic DNA extracted from LCLs as follows. LCLs were lysed with genomic DNA extraction buffer (100 mM Tris-HCl pH8.0, 5 mM EDTA, 0.2% SDS, 200 mM NaCl and 200 μg/mL proteinase K) and the lysate was incubated at 50°C for 3 hr. After phenol-chloroform extraction, genomic DNA was purified by ethanol precipitation procedure. A 121-bp fragment of the EBV W repeat region was amplified by the forward primer 5′-CGCATAATGGCGGACCTAG-3′ and reverse primer 5′-CAAACAAGCCCACTCCCC-3′ in a 25 μl reaction mixture comprising 1 × AmpliTaq Gold buffer, 3.5 mM MgCl2, 200 μM dNTP, 300 nM primers, 200 nM probe and 0.025 U/μl AmpliTaq Gold. The PCR cycle conditions were as follows: a DNA denaturation and polymerase activation step of 10 min at 95°C and then 40 cycles of amplification (95°C for 15 sec, 60°C for 1 min). PCR products were separated by electrophoresis on agarose gels, stained with ethidium bromide and visualized by UV-light.

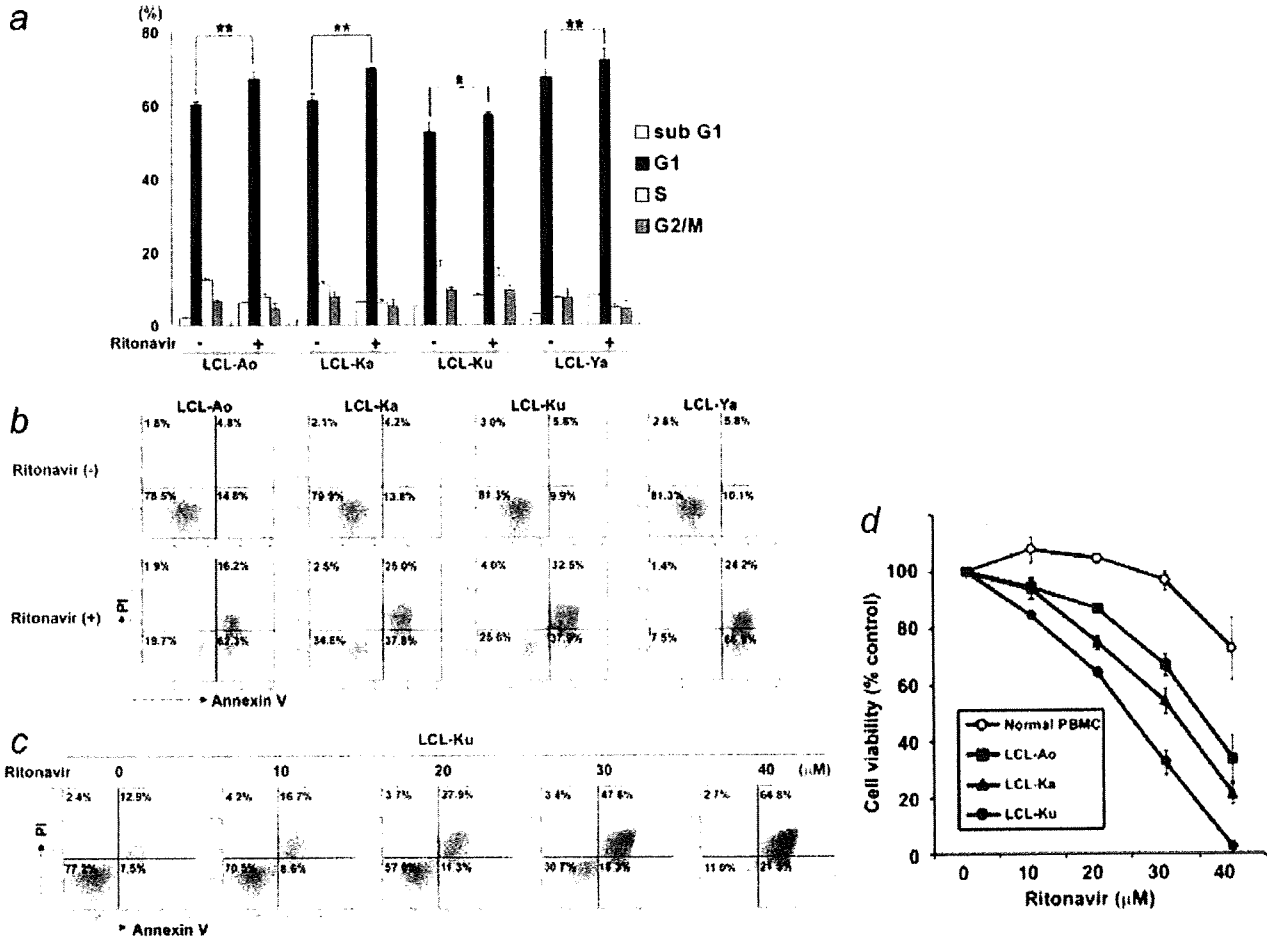

FIGURE 1 – Effect of ritonavir on cell cycle arrest and induction of apoptosis of EBV-positive lymphoblastoid B cells. (*a*) Effect of ritonavir on cell cycle progression of EBV-positive lymphoblastoid B cells. Cells were cultured for 24 hr with (+) or without (−) ritonavir (40 μM). DNA content was analyzed by flow cytometry with PI staining. Sub G_1, S and G_2/M indicate the stages of the cell cycle. Data are expressed as the mean percentages of the cells from three independent experements. Significance of differences between % G_1 of ritonavir treated (+) and untreated (−) cells calculated by Student's *t*-test is shown as *P*-value with astalisk(s). $*p < 0.05$ and $**p < 0.01$. (*b*) Effect of ritonavir on induction of apoptosis of EBV-immortalized B-cell lines. Cells were cultured for 72 hr with (+) or without (−) ritonavir (40 μM). (*c*) Ritonavir induces apoptosis of EBV-immortalized B-cell lines in a dose-dependent manner. LCL-Ku cells were cultured for 72 hr with increasing concentration of ritonavir (0, 10, 20, 30, 40 μM). Cells were harvested and stained with Annexin-V and PI. Apoptosis was analyzed by flow cytometry. Bottom left quadrants, viable cells; bottom right quadrants, early apoptotic cells. Top right quadrants, nonviable, late apoptotic/necrotic cells. (*d*) Effect of ritonavir on cell viability of LCLs and PBMCs from normal healthy controls. LCLs and PBMCs were incubated in the presence of various concentrations of ritonavir for 72 hr and viability of the cultured cells was measured by WST-8 assay. Relative viability of the cultured cells is presented as the mean determined on LCLs and PBMCs from triplicate cultures. A relative viability of 100% was designated as total number of cells that grew in 72-hr cultures in the absence of ritonavir.

Treatment of tumor-bearing mice with ritonavir

Ritonavir was obtained from Abbott Labs, North Chicago, IL. LCL-Ku cells (1×10^7) were inoculated s.c. in the post-auricular region of NOG mice. The drug was administered s.c. into the tumor cells inoculated site of mice at doses of 30 mg/kg/day, beginning on day 0 for 3 weeks. The control mice received RPMI-1640 (200 μl) simultaneously. In other experiments, ritonavir or RPMI-1640 was also administered intraperitoneally into mice as the same doses stated above, beginning on day 4 for 18 days.

In situ *hybridization*

EBERs were detected by *in situ* hybridization using fluorescein isothiocyanate (FITC)-conjugated EBER PNA (peptide nucleic acid)-probe (DAKO). Briefly, formalin-fixed, paraffin-embedded tissue sections of tumor and various organs were deparaffinized and hydrated in xylenes and graded alcohol series, then rinsed for 5 min in PBS. Deparaffinized samples were incubated with 10 ng/μl of proteinase K for 20 min at 37°C followed by washing, and then incubated with 0.3% methanol for 30 min at room temperature. After washing in PBS, the sections were hybridized with FITC-conjugated EBER-PNA probe in the hybridization solution for 90 min at 56°C. The slides were washed twice in 0.2 × SSC for 20 min at 56°C, and incubated with anti-FITC monoclonal antibody (DAKO) for 45 min at 37°C. Followed by washing, the slides were incubated with horse-radish peroxidase-conjugated polymer reagent (Envision, DAKO) for 30 min at room temperature. Positive staining was visualized after incubation of these samples with a mixture of 0.05% 3,3′-diaminobenzidine tetrahydrochloride in 50 mM Tris-HCl buffer pH7.6 and 0.01% hydrogen peroxide for 5 min. The samples were counterstained with hematoxlin for 2 min, hydrated completely, cleaned in xylene and then mounted. The samples were visualized and photographed under light microscopy (BX41 and DP70; Olympus, Tokyo, Japan).

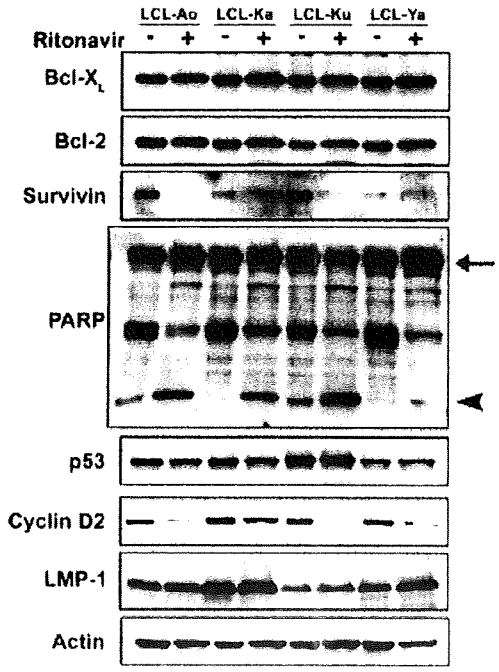

FIGURE 2 – Ritonavir inhibits expression of apoptosis- and cell cycle-associated proteins. EBV-immortalized B-cell lines were cultured with (+) or without (−) ritonavir (40 μM) for 24 hr. Cells were harvested and subjected to Western blot analysis. The polyvinylidene fluoride membrane was sequentially probed with indicated antibodies. Arrow indicates full-length PARP (116 kDa) and arrow head indicates cleaved form of PARP (25 kDa). Essentially the same results were obtained in 3 experiments and representative data are shown.

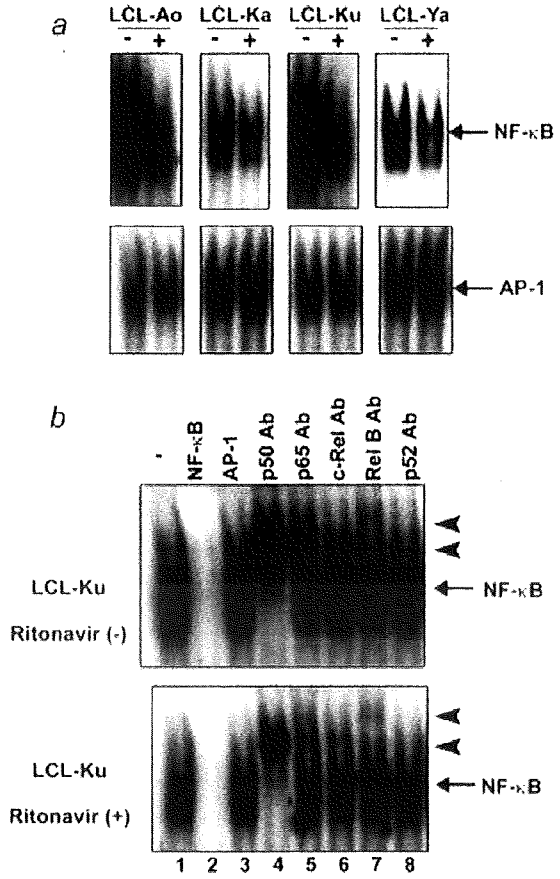

FIGURE 3 – Ritonavir inhibits constitutive NF-κB activation. (*a*) EBV-immortalized B-cell lines were cultured with (+) or without (−) ritonavir (40 μM) for 24 hr and assessed for NF-κB and AP-1-DNA binding activity. (*b*) Cold competition using 100-fold excess of unlabeled NF-κB oligonucleotide, or AP-1 oligonucleotide (lanes 2–3) demonstrated the specificity of the protein/DNA binding complexes. Specificity of NF-κB binding was also determined by using antibodies to the NF-κB components p50, p65, c-Rel, RelB and p52, resulting in supershift (lanes 4–8). Arrows indicate specific complexes of NF-κB with wild type NF-κB oligonucleotide. Arrow heads indicate supershift. Essentially the same results were obtained in 3 experiments and representative data are shown.

Results

Ritonavir induces cell-cycle arrest and apoptosis of LCLs

Ritonavir was examined for its effect on cell-cycle distribution of EBV-immortalized LCLs (Fig. 1*a*). Ritonavir effectively inhibited cell-cycle progression, as evidenced by increased proportion of the cells in G_1 phase of LCL-Ao, LCL-Ka, LCL-Ku and LCL-Ya (LCL-Ao: from 60.1% to 67.1%; LCL-Ka: from 61.2% to 69.9%; LCL-Ku: from 52.6% to 57.3%; and LCL-Ya: from 67.4% to 72.1%). These results indicated that ritonavir induced cell-cycle arrest at G_1-phase. The weak accumulation of cells in G_1 phase by ritonavir suggests that it might rather be an apoptosis inducer than a cell growth inhibitor.

Furthermore, we evaluated the effect of ritonavir on the cell viability of LCLs and PBMCs from healthy individuals (Fig. 1*d*). Ritonavir effectively reduced the survival of LCLs (LCL-Ao, LCL-Ka and LCL-Ku) as measured by WST-8 on the third day of culture in a dose-dependent manner. In contrast, ritonavir hardly affected the survival of PBMCs from healthy volunteers.

The effect of ritonavir on apoptosis was examined by the Annexin-V and PI method. Annexin-V binds to the cells that express phosphatidylserine on the outer layer of the cell membrane, a characteristic feature of cells entering apoptosis. Early apoptotic cells were stained with Annexin V but not with PI. Late apoptotic and necrotic cells were stained with both fluorescent. Ritonavir induced increased proportion of cells positive for Annexin-V and negative for PI in all cell lines (LCL-Ao: from 14.8% to 62.3%; LCL-Ka: from 13.8% to 37.8%; LCL-Ku: from 9.9% to 37.9% and LCL-Ya: from 10.1% to 66.9%) (Fig. 1*b*). Ritonavir also induced dose-dependent increasing of Annexin-V positive and PI negative cells in LCL-Ku cells (Fig. 1*c*), indicating increasing apoptosis of ritonavir-treated cells.

Ritonavir down-regulates the expression of the cell-cycle- and apoptosis-associated genes

The antiproliferative and proapoptotic effects of ritonavir were explored by examining the levels of intracellular regulators of cell-cycle and apoptosis after exposure to ritonavir (Fig. 2). Ritonavir down-regulated the levels of survivin and cyclin D2 in EBV-immortalized B-cell lines. We also observed increased cleavage of PARP in these cells. However, ritonavir did not modulate the other regulators of cell-cycle and apoptosis such as Bcl-X_L, Bcl-2 and p53. Ritonavir had no effect on the expression of viral proteins such as LMP-1, suggesting that ritonavir may induce cell-cycle arrest and apoptosis by down-regulating the levels of survivin and cyclin D2 without reducing the virus levels in the cells.

Ritonavir suppresses constitutive NF-κB expressed by EBV-transformed LCLs

To examine the effect of ritonavir on NF-κB DNA binding, EMSA was performed. EBV-immortalized B-cell lines were incubated with or without 40 μM ritonavir for 24 h, and nuclear extracts were prepared and examined for NF-κB by EMSA.

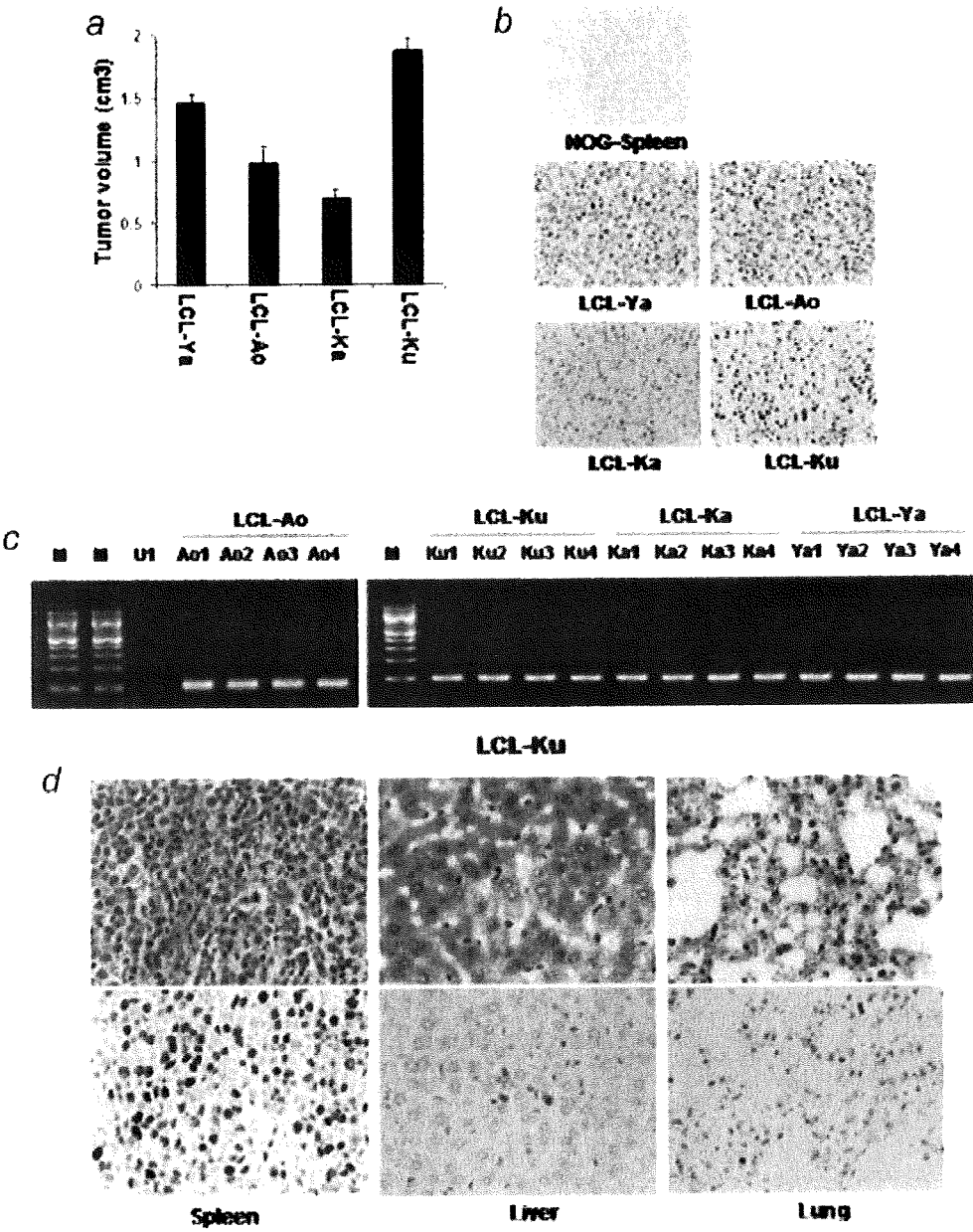

FIGURE 4 – Successful engraftment and infiltration of EBV-positive lymphoblastoid B cells in NOG mice. (*a*) Subcutaneous tumor size in mice 21 days after inoculation with various LCL cells. (*b*) *In situ* hybridization for EBER of spleen from NOG mice not receiving tumor cells, as a negative control and tumor tissues of LCL cells injected mice. Magnification ×40. (*c*) Detection of viral DNA by PCR. M, Marker; U1; EBV-negative U937 cell for negative control; Ao1, *in vitro* culture and Ao2, Ao3 and Ao4, *in vivo* samples from 3 different mice inoculated with LCL-Ao; Ku1, *in vitro* culture and Ku2, Ku3 and Ku4, *in vivo* sample from 3 different mice inoculated with LCL-Ku; Ka1, *in vitro* culture and Ka2, Ka3 and Ka4, *in vivo* sample from 3 different mice inoculated with LCL-Ka, Ya1, *in vitro* culture and Ya2, Ya3 and Ya4, *in vivo* sample from 3 different mice inoculated with. LCL-Ya. Infiltration of EBV-immortalized B-cell lines in various organs of NOG mice. (*d*) HE and *in situ* hybridization for EBER of spleen, liver and lung of mice inoculated with LCL-Ku cells. Left, middle and right panels represent spleen, liver and lung, respectively. Upper and lower panels represent HE and EBER, respectively (magnification ×40).

Down-regulation of NF-κB occurred in all cell lines (Fig. 3*a*, upper panels). Inhibition appeared specific to NF-κB, because no significant change in binding activity of AP-1 was observed after treatment of cells with ritonavir (Fig. 3*a*, lower panels). Also, the observed protein/DNA binding was specific for NF-κB, because the binding was effectively competed and abrogated by excess unlabeled NF-κB oligonucleotide but not by mutant NF-κB or AP-1 oligonucleotide (Fig. 3*b*). LCL-Ku cell extract without ritonavir treatment contained p50, p65 and Rel B proteins in the NF-κB complex (Fig. 3*b*, upper panel), and ritonavir did not affect components of the NF-κB complex (Fig. 3*b*, lower panel).

Efficient engraftment and infiltration of EBV-transformed LCLs in NOG mice

EBV-immortalized LCLs (LCL-Ya, LCL-Ao, LCL-Ka and LCL-Ku) were inoculated s.c. in the post-auricular region of NOG mice (Fig. 4 and Table I). Mice inoculated with LCL cells (LCL-

TABLE I – *IN VIVO* CHARATERISTICS OF EBV-POSITIVE LYMPHOBLASTOID B CELLS IN NOG MICE

Cell line	Orgin/EBV status	No. of cells inoculated/mouse (10^7)[1]	Inoculation route[2]	Day of sacrifice after inoculation	No. of mice with tumor/no. of mice inoculated[3]	Organ-infiltration[4]		
						Spleen	Liver	Lung
LCL-Ya	B/+	1	sc	21	03/03	++	–	–
LCL-Ao	B/+	1	sc	21	03/03	++	–	–
LCL-Ka	B/+	1	sc	21	03/03	++	–	–
LCL-Ku	B/+	1	sc	21	21/21	+++	+	+

[1]Mice were inoculated with 1×10^7 cells per mouse.–[2]sc, subcutaneous.–[3]Number of animals in which tumor developed.–[4]Organ-infiltration was examined by histological analysis.–, no infiltration; +, slight infiltration; ++, marked infiltration; +++, massive infiltration.

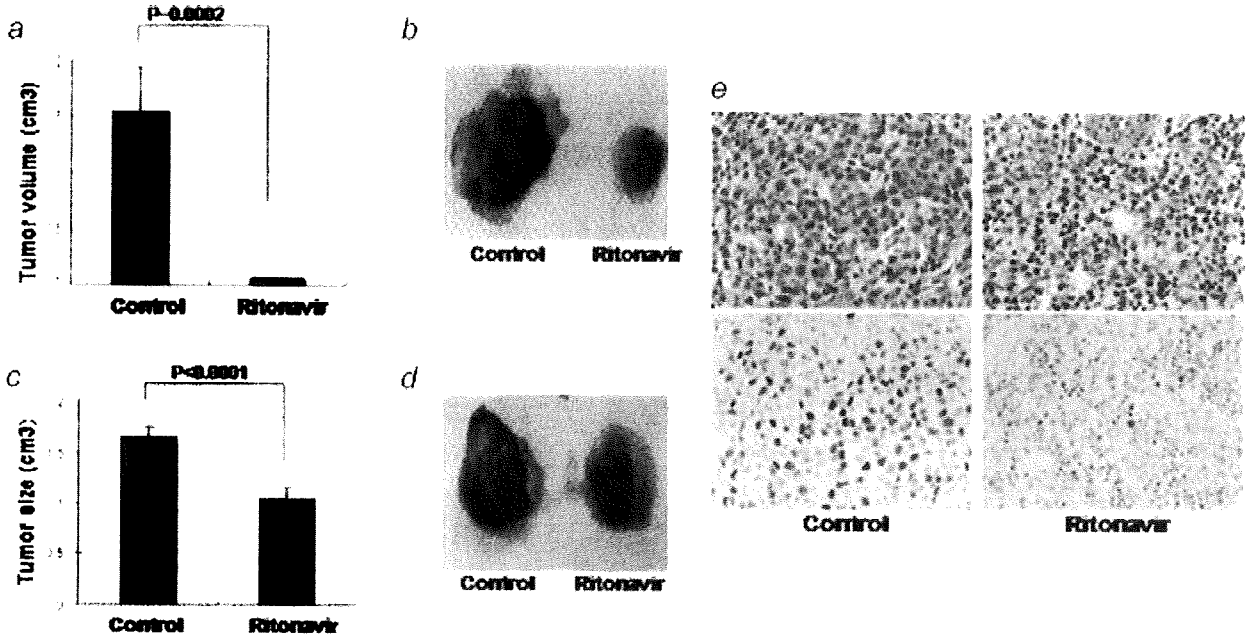

FIGURE 5 – Effect of ritonavir on lymphoma cell growth and infiltration. Mice were injected with LCL-Ku cells (1×10^7 cells) s.c. in the postauricular region. (*a* and *b*) The drug was administered s.c. into the tumor cells inoculated site of mice at doses of 30 mg/kg/day, beginning on day 0 for 3 weeks. The control mice received RPMI-1640 (200 µl) simultaneously. (*a*) Average size of tumor, data represent the mean ± SD from 6 mice. (*b*) Photograph of subcutaneously formed excised tumor without (left) and with (right) ritonavir treatment. (*c* and *d*) Effect of ritonavir on established tumor, ritonavir or RPMI-1640 was also administered intraperitoneally into mice as the same doses stated above, beginning on day 4 for 18 days. (*c*) Average size of tumor, data represent the mean ± SD from 6 mice. (*d*) Photograph of subcutaneously formed excised tumor without (left) and with (right) ritonavir treatment. (*e*) HE and *in situ* hybridization for EBER in spleen tissue of LCL cells injected mice. Magnification ×40. Upper and lower panels show HE and EBER staining, respectively.

Ya, LCL-Ao, LCL-Ka and LCL-Ku) produced a visible tumor within 3 weeks in all NOG mice. LCL-Ku cell was very efficient in the formation of a large tumor (Fig. 4*a*), as well as development of clinical signs of near-death, such as pilorection, weight loss and cachexia in mice at the time point of sacrifice. The average tumor size (LCL-Ya, LCL-Ao, LCL-Ka and LCL-Ku) in NOG mice inoculated s.c. with lymphoma cells was shown in Figure 4*a*. To test whether tumors maintain original histomorphology and expression patterns of tumor markers in NOG, we performed HE and *in situ* hybridization for EBER of normal mice spleen not receiving tumor cells and tumor tissues obtained from mice inoculated with LCLs. Histological analysis revealed that morphologically immunoblastic cells with large nucleus, clear nuclear membrane and broad cytoplasm expressed EBER, whereas EBER was not detected in spleen tissue collected from mice not receiving tumor cells, suggesting that *in vivo* tumor cells preserved well morphology as well as expressed viral gene EBER (Fig. 4*b*). Tumor cells from mice inoculated with EBV-immortalized B-cell lines were positive for DNA of EBV by PCR (Fig. 4*c*). These results showed that EBV-immortalized B-cell lines inoculated s.c. into the postauricular region of NOG mice were able to produce a visible tumor very efficiently. To assess the tissue distribution of lymphoma cells, we carried out histological examinations of the different organs of NOG mice after inoculation of the cells. Proliferation and infiltration of tumor cells were found not only in primary tumor tissues but also in spleen and to a lesser extent in liver and lung of NOG mice inoculated with tumor cells (Table I). HE and *in situ* hybridization staining for EBER showed a degree of infiltration of tumor cells at the site of inoculation and various organs with lymphoma cells (Fig. 4*d*). Interestingly, LCL-Ku cells appeared to infiltrate in various organs of mice more aggressively and massively than other cells. This extremely rapid tumor formation and infiltration in all mice is one of the hallmarks of our clinically relevant animal model without change of histomorphology or tumor marker expression.

Ritonavir suppresses the LCLs growth and infiltration in vivo

To determine the effect of ritonavir on tumor growth and infiltration, we injected LCL-Ku cells (1×10^7) s.c. into the postauricular region of NOG mice. Mice were treated with either RPMI-1640 (as control) or ritonavir (30 mg/kg/day), beginning on either day 0 or day 4. A significant decrease in the size of tumors in mice treated with ritonavir was demonstrated when compared with controls 3 weeks after the injection of tumor cells (Fig. 5*a*). Gross appearance of the mice treated by ritonavir showed apparent

reduction of the tumor mass at 3 weeks after inoculation of tumor cells (Fig. 5*b*). Ritonavir also inhibited the size and growth of established tumors (Fig. 5*c* and 5*d*). Ritonavir at this treatment dosage (30 mg/kg/day for 3 weeks) is well tolerated without adverse findings such as standing of hair, weight loss and cachexia of treated mice, all of which are signs of near death. Clinical evaluation of organ invasion 3 weeks after injection of tumor cells showed that ritonavir treatment inhibited their infiltration into spleen (Fig. 5*e*). In contrast, all control mice showed infiltration with tumor cells into spleen. Organ infiltration of lymphoma cells were analyzed and evaluated by HE and *in situ* hybridization of EBER. Together, these data indicate that ritonavir significantly inhibits lymphoma cell growth and infiltration in various organs of NOG mice (Fig. 5).These results suggest that ritonavir contributes to the reduction of the tumor growth and inhibits the organ infiltration in the mice through targeting the constitutive NF-κB activity.

Discussion

EBV-positive malignancies in immunocompromised patients are associated with high mortality and reduce overall survival period. The various chemotherapies so far developed have not increased significantly the survival of patients with EBV-associated malignancies in immunocompromised patients. Given disappointing results using conventional chemotherapy, new treatment strategies that specially target EBV-transformed cells are need.[1,2] LMP-1 is an oncogene that constitutively activates NF-κB to induce B cell proliferation.[7] It has been previously reported that suppression of high NF-κB activity inhibited cell growth and induced apoptosis of cancer cells as well as EBV-transformed cells both *in vitro* and *in vivo*.[12–20,33] Ritonavir is cytotoxic for different types of malignant cells *in vitro* through affecting proteasomal proteolysis, although concentrations necessary to show the *in vitro* effect exceed the achievable therapeutic drugs level.[27,29,30] It may affect the stabilization of p21, p27 and p53 proteins. Recently, ritonavir has been shown to inhibit NF-κB activity and induce the apoptosis of ATL cells.[20] This led us to investigate whether this drug exhibits anti-tumor effects against EBV-transformed cells *in vitro* and in our preclinical murine model. In the present study, we established a unique murine model that presents aggressive features concerning cell growth and infiltration in SCID mice within 3 weeks. Thus, it represents a novel model to evaluate tissue toxicity and the efficacy of therapeutic agents directed toward the treatment of EBV-associated lymphoproliferative diseases.

The blood-plasma ritonavir concentrations obtained in the therapy of HIV-infection are between 5 to 15 μM,[34] but much higher maximal concentrations (up to 46 μM) have been demonstrated in individual patients.[35] In the present study, we used the concentration of ritonavir for doing *in vitro* experiments from 0 to 40 μM and *in vivo* 30 mg/kg/day used for treatment of AIDS patients. Constitutive and strong NF-κB activation was reported to be a characteristic of LCL and important for LCL growth and survival.[7] Our results indicate that inhibition of NF-κB activity by ritonavir reduced cell growth and induced apoptosis of these cells. This is consistent with down-modulation of NF-κB regulated genes such as antiapoptotic and cell-cycle related genes. Our murine model clearly indicate that 30 mg/kg/day of ritonavir (the same dose used clinically for treating HIV/AIDS patients) significantly inhibits EBV-transformed cell growth and infiltration into various organs of NOG mice. The plasma exposure produced by this dose in mice is only approximately one-half of the plasma exposure observed with the licensed dose of ritonavir in human (600 mg BID). In our murine model, ritonavir at this treatment dosage is well tolerated without severe adverse effects observed in the mice during the treatment period. These data strongly suggest that the HIV protease inhibitor, ritonavir, is a promising antitumor agent against EBV-transformed cells and could be used clinically for treatment of EBV-associated malignancies. These results suggest that anti-tumor activity of ritonavir correlates with suppression of NF-κB activity.

In summary, we have established a novel NOG EBV-associated lymphoma model that presents features similar to patients with EBV-infection in immunocompromised patients. These results also indicate that the HIV protease inhibitor, ritonavir, showed antitumor and anti-NF-κB activity against EBV-transformed cells. Finally, our results strongly suggest that NF-κB serves as a potential molecular target to treat EBV-associated malignancies, and that ritonavir might be used clinically as a single compound or in combination with the reducing dose of chemotherapeutic agents for treatment of patients with life-threatening EBV-associated lymphoproliferative diseases and AIDS-associated lymphomas.

Acknowledgements

We thank D. Kempf and T. Yamada of Abbott Laboratories, S. Ichinose of Instrumental Analysis Research Center and S. Endo of Animal Research Center, Tokyo Medical and Dental University for their advice and assistance with the experiments. We also thank Y. Sato of the National Institute of Infectious Diseases for her excellent technical assistance.

References

1. Rickinson AB, Kieff E. Epstein-Barr virus. In: Fields BN, ed. Fields virology, 4th edn. New York (NY): Lippincott Williams and Wilkins, 2001. Vol. 1, 2575–627.
2. Kieff E, Rickinson AB. Epstein-Barr virus and replication. In: Fields BN, ed. Fields virology, 4th ed. New York (NY): Lippincott Williams and Wilkins, 2001. Vol. 1, 2511–73.
3. Zur Hausen H, Schulte-Holthausen H. Presence of EB virus nucleic acid homology in a "virus-free" line of Burkitt tumour cells. Nature 1970;227:245–48.
4. Nonoyama M, Pagano JS. Homology between Epstein-Barr virus DNA and viral DNA from Burkitt's lymphoma and nasopharyngeal carcinoma determined by DNA-DNA reassociation kinetics. Nature 1973;242:44–7.
5. Rowe M, Lear AL, Croom-Carter D, Davies AH, Rickinson AB. Three pathways of Epstein-Barr virus gene activation from EBNA1-positive latency in B lymphocytes. J Virol 1992;66:122–31.
6. Yamamoto N, Takizawa T, Iwanaga Y, Shimizu N, Yamamoto N. Malignant transformation of B lymphoma cell line BJAB by Epstein-Barr virus-encoded small RNAs. FEBS Lett 2000;484:153–58.
7. Mosialos G, Birkenbach M, Yalamanchili R, VanArsdale T, Ware C, Kieff E. The Epstein-Barr virus transforming protein LMP1 engages signaling proteins for the tumor necrosis factor receptor family. Cell 1995;80:389–99.
8. Mori N, Fujii M, Ikeda S, Yamada Y, Tomonaga M, Ballard DW, Yamamoto N. Constitutive activation of NF-κB in primary adult T-cell leukemia cells. Blood 1999;93:2360–8.
9. Baldwin AS. The NF-κB and IκB proteins: new discoveries and insights. Annu Rev Immunol 1999;14:649–81.
10. Guinness ME, Kenney JL, Reiss M, Lacy J. Bcl-2 antisense oligodeoxynucleotide therapy of Epstein-Barr virus-associated lymphoproliferative disease in severe combined immunodeficient mice. Cancer Res 2000;60:5354–8.
11. Miyake A, Dewan MZ, Ishida T, Watanabe M, Honda M, Sata T, Yamamoto N, Umezawa K, Watanabe T, Horie R. Induction of apoptosis in Epstein-Barr virus-infected B-lymphocytes by the NF-kappaB inhibitor DHMEQ. Microbes Infect 2008;10:748–56.
12. Watanabe M, Dewan MZ, Okamura T, Sasaki M, Itoh K, Higashihara M, Mizoguchi H, Honda M, Sata T, Watanabe T, Yamamoto N, Umezawa K, et al. A novel NF-κB inhibitor DHMEQ selectively targets constitutive NF-κB activity and induces apoptosis of multiple myeloma cells in vitro and in vivo. Int J Cancer 2005;114:32–8.
13. Adams J, Palombella VJ, Elliott PJ. Proteasome inhibition: a new strategy in cancer treatment. Invest New Drugs 2001;18:109–21.
14. Teicher BA, Ara G, Herbst R, Palombella VJ, Adams J. The proteasome inhibitor PS-341 in cancer therapy. Clin Cancer Res 1999; 5:2638–45.

15. Hideshima T, Chauhan D, Richardson P, Mitsiades C, Mitsiades N, Hayashi T, Munshi N, Dang L, Castro A, Palombella V, Adams J, Anderson KC. NF-κB as a therapeutic target in multiple myeloma. J Biol Chem 2002;277:16639–47.
16. Dewan MZ, Terashima K, Taruishi M, Hasegawa H, Ito M, Tanaka Y, Mori N, Sata T, Koyanagi Y, Maeda M, Kubuki Y, Okayama A, et al. Rapid tumor formation of human T-cell leukemia virus type 1-infected cell lines in novel NOD-SCID/γc^{null} mice: suppression by an inhibitor against NF-κB. J Virol 2003;77:5286–94.
17. Kitajima I, Shinohara T, Bilakovics J, Brown DA, Xu X, Nerenberg M. Ablation of transplanted HTLV-I Tax-transformed tumors in mice by antisense inhibition of NF-κB. Science 1992;258:1792–5.
18. Mori N, Yamada Y, Ikeda S, Yamasaki Y, Tsukasaki K, Tanaka Y, Tomonaga M, Yamamoto N, Fujii M. Bay 11–7082 inhibits transcription factor NF-κB and induces apoptosis of HTLV-I-infected T-cell lines and primary adult T-cell leukemia cells. Blood 2002;100:1828–34.
19. Tan C, Waldmann TA. Proteasome inhibitor PS-341, a potential therapeutic agent for adult T-cell leukemia. Cancer Res 2002;62: 1083–6.
20. Dewan MZ, Uchihara JN, Terashima K, Honda M, Sata T, Ito M, Fujii N, Uozumi K, Tsukasaki K, Tomonaga M, Kubuki Y, Okayama A, et al. Efficient intervention of growth and infiltration of primary adult T-cell leukemia cells by an HIV protease inhibitor, ritonavir. Blood 2006;107:716–24.
21. Cahir-McFarland ED, Davidso DM, Schauer SL, Duong J, Kieff E. NF-kappa B inhibition causes spontaneous apoptosis in Epstein-Barr virus-transformed lymphoblastoid cells. Proc Natl Acad Sci USA 2000;97:6055–60.
22. Collier AC. Efficacy of combination antiretroviral therapy. Adv Exp Med Biol 1996;394:355–72.
23. Collier AC, Coombs RW, Schoenfeld DA, Bassett R, Baruch A, Corey L. Combination therapy with zidovudine, didanosine and saquinavir. Antiviral Res 1996;29:99.
24. Collier AC, Coombs RW, Schoenfeld DA, Bassett RL, Timpone J, Baruch A, Jones M, Facey K, Whitacre C, McAuliffe VJ, Friedman HM, Merigan TC, et al. Treatment of human immunodeficiency virus infection with saquinavir, zidovudine, and zalcitabine. AIDS Clinical Trials Group. N Engl J Med 1996;334:1011–17.
25. Markowitz M, Saag M, Powderly WG, Hurley AM, Hsu A, Valdes JM, Henry D, Sattler F, La Marca A, Leonard JM, Ho DD. A preliminary study of ritonavir, an inhibitor of HIV-1 protease, to treat HIV-1 infection. N Engl J Med 1995;333:1534–39.
26. Kempf DJ, Marsh KC, Denissen JF, McDonald E, Vasavanonda S, Flentge CA, Green BE, Fino L, Park CH, Kong XP, Wideburg NE, Saldivar A, et al. ABT-538 is a potent inhibitor of human immunodeficiency virus protease and has high oral bioavailability in humans. Proc Natl Acad Sci USA 1995;92:2484–88.
27. Andre P, Groettrup M, Klenerman P, de Giuli R, Booth BL, Jr, Cerundolo V, Bonneville M, Jotereau F, Zinkernagel RM, Lotteau V. An inhibitor of HIV-1 protease modulates proteasome activity, antigen presentation, and T cell responses. Proc Natl Acad Sci USA 1998; 95:13120–24.
28. Liang JS, Distler O, Cooper DA, Jamil H, Deckelbaum RJ, Ginsberg HN, Sturley SL. HIV protease inhibitors protect apolipoprotein B from degradation by the proteasome: a potential mechanism for protease inhibitor-induced hyperlipidemia. Nat Med 2001;7:1327–31.
29. Schmidtke G, Holzhütter HG, Bogyo M, Kairies N, Groll M, de Giuli R, Emch S, Groettrup M. How an inhibitor of the HIV-I protease modulates proteasome activity. J Biol Chem 1999;274:35734–40.
30. Gaedicke S, Firat-Geier E, Constantiniu O, Lucchiari-Hartz M, Freudenberg M, Galanos C, Niedermann G. Antitumor effect of the human immunodeficiency virus protease inhibitor ritonavir: induction of tumor-cell apoptosis associated with perturbation of proteasomal proteolysis. Cancer Res 2002;62:6901–8.
31. Pati S, Pelser CB, Dufraine J, Bryant JL, Reitz JMS, Weichold FF. Antitumorigenic effects of HIV protease inhibitor ritonavir: inhibition of Kaposi sarcoma. Blood 2002;99:3771–9.
32. Sgadari C, Barillari G, Toschi E, Carlei D, Bacigalupo I, Baccarini S, Palladino C, Leone P, Bugarini R, Malavasi L, Cafaro A, Falchi M, et al. HIV protease inhibitors are potent anti-angiogenic molecules and promote regression of Kaposi sarcoma. Nat Med 2002;8:225–32.
33. Katano H, Pesnicak H, Cohen JI. Simvastatin induces apoptosis of Epstein-Barr virus (EBV)-transformed lymphoblastoid cell lines and delays development of EBV lymphomas. Proc Natl Acad Sci USA 2004;101:4960–5.
34. Norvir. Ritonavir Product monograph. North Chicago, IL: Abbott laboratories, 1997.
35. Gatti G, Di Biagio A, Casazza R, De Pascalis C, Bassetti M, Cruciani M, Vella S, Bassetti D. The relationship between ritonavir plasma levels and side-effects: implications for therapeutic drug monitoring. AIDS 1999;13:2083–9.

International Immunology, Vol. 21, No. 7, pp. 843–858
doi:10.1093/intimm/dxp050

The analysis of the functions of human B and T cells in humanized NOD/shi-scid/γc^{null} (NOG) mice (hu-HSC NOG mice)

Yohei Watanabe[1,2], Takeshi Takahashi[1], Akira Okajima[1], Miho Shiokawa[1], Naoto Ishii[1], Ikumi Katano[3], Ryoji Ito[3], Mamoru Ito[3], Masayoshi Minegishi[4], Naoko Minegishi[5], Shigeru Tsuchiya[2] and **Kazuo Sugamura[1]**

[1]Department of Microbiology and Immunology and [2]Department of Pediatrics, Tohoku University Graduate School of Medicine, 2-1 Seiryo-cho, Aoba-ku, Sendai 980-8575, Japan
[3]Laboratory of Immunology, Central Institute for Experimental Animals, 1430 Nogawa, Miyamae-ku, Kawasaki 216-0001, Japan
[4]Division of Blood Transfusion, Tohoku University Hospital, 2-1 Seiryo-cho, Aoba-ku, Sendai 980-8575, Japan
[5]Department of Health and Welfare Science, Sendai University, 2-2-18 Funaokaminami, Shibata-machi, Miyagi-ken 989-1693, Japan

Keywords: adaptive immunity, humanized mice, NOG mice, thymus

Abstract

'Humanized mice' are anticipated to be a valuable tool for studying the human immune system, but the reconstituted human immune cells have not yet been well characterized. Here, we extensively investigated the differentiation and functions of human B and T cells in a supra-immunodeficient mouse strain, NOD/shi-scid/γc^{null} (NOG) reconstituted with $CD34^+$ hematopoietic stem cells obtained from umbilical cord blood. In these hu-HSC NOG mice, the development of human B cells was partially blocked, and a significant number of B-cell progenitors accumulated in the spleen. The mature $CD19^+IgM^+IgD^+$ human B cells of the hu-HSC NOG mice could produce IgG *in vivo* and *in vitro* by antigenic stimulation. In contrast, although human T cells with an apparently normal phenotype developed, most of them could neither proliferate nor produce IL-2 in response to antigenic stimulation by anti-CD3 and anti-CD28 antibodies *in vitro*. The positive selection of human T cells in the thymus was sufficiently functional, if not complete, and mainly mediated by mouse class II, suggesting that the human T cells lost their function in the periphery. We found that multiple mechanisms were involved in the T-cell abnormalities. Collectively, our results demonstrate that further improvements are necessary before humanized mice with a functional human immune system are achieved.

Introduction

Recently, human immunity research has increased in momentum, owing largely to accumulating evidence that human immunity can be inferred from animal models. However, the extent to which these models directly reflect the human immune system is still open to question. For example, genetic abnormalities often lead to different phenotypes in different species (i.e. patients with spontaneous mutations in a certain gene and the corresponding gene-disrupted mice), resulting in complicated interpretations about the human immune system (1–3). In addition, different responses to pharmacological reagents developed in animals can result in unexpected adverse effects when they are used for therapeutic treatments (4). Hence, the development of novel model systems in which the human immune system can be functionally studied in a reliable manner without various constraints is desired not only for understanding human immunity but also for improving 'translational' research.

'Humanized mice' have been considered one such model (5–9). For the past two decades, many studies have attempted to graft immunodeficient animals with human tissues or cells (10–12). In particular, the inoculation of human hematopoietic cells or PBMCs has been frequently performed to examine whether even a part of the functional human immune system can be reconstituted. Although various immunodeficient mice, including athymic nude mice (*nu/nu*), C.B.-17 *scid* mice, and NOD/SCID mice, have been used as recipients (10–12), there

Correspondence to: T. Takahashi; E-mail: takeshi-takahashi@mail.tains.tohoku.ac.jp

Transmitting editor: K. Yamamoto

Received 13 March 2009, *accepted* 1 May 2009
Advance Access publication 10 June 2009

seem to be major obstacles to the xenotransplantations. For example, the simple transfer of human PBMCs into such immunodeficient animals results in the failure of stable engraftment, the functional impairment of the donor cells and in some cases the uncontrolled activation of human T cells against mouse tissues (xenogenic graft versus host disease) (13, 14). In addition, when human $CD34^+$ hematopoietic stem cells are transferred, the reconstitution of human immune cells is often incomplete, as revealed by a lack of T-cell development in reconstituted NOD/SCID mice (15). Furthermore, the poor graft survival of human hematopoietic stem cells makes it difficult to perform long-term experiments (16). These limitations have hampered the research on human immune systems in humanized mice.

The recent development of a new immunodeficient strain, however, has opened up the possibility for generating better xenotransplantation systems (5, 6, 16). Disruption of the IL-2R γ chain (γc) produces a mouse strain deficient for B, T, NK and NKT cells since the signalings through γc of multiple cytokines (IL-2, IL-4, IL-7, IL-15, etc.) are indispensable for the development of a wide range of immune cell lineages (17–19). By backcrossing the γc knockout (KO) mice onto the NOD background, which has low endogenous NK activity, and introducing the *scid* mutation, the NOD/Shi-scid-IL-2Rγ $(\gamma c)^{null}$ (NOG) strain was generated (16, 20, 21). As a consequence, NOG mice have almost no functional endogenous immune system. Using NOG or the similar BALB-RAG2/γc double-KO mice, several groups have reported a more efficient and stable reconstitution of human hematopoietic cells than was previously possible, using human $CD34^+$ stem cells from various sources, including bone marrow (BM), umbilical cord blood or peripheral blood immobilized by granulocyte colony stimulating factor (16, 20–22). For example, such humanized mice harbor human $CD34^+$ stem cells in their BM for up to 1 year, and the cells can be serially transferred into new recipients to reconstitute them (16). In addition, apparently normal human B and T cells or their progenitors are found in the spleen or BM, respectively (16, 20, 21), and major subsets of human hematopoietic cells have been successfully developed from these mice (22, 23). Hence, these supra-immunodeficient strains are presently considered the most suitable for reconstituting quasi-human immune systems.

Nevertheless, it is also clear that there is room for improvement in the present humanized mouse technology. For example, upon exogenous antigenic challenge, humanized mice (hu-HSC-NOG mice) produce abundant antigen-specific IgM antibodies, but little antigen-specific IgG (21, 22, 24, 25). This predominant IgM production suggests that only a partial reconstitution of the human adaptive immune system is achieved in the hu-HSC-NOG mice. In the present study, we sought to identify critical cues for recapitulating functional human immunity in hu-HSC-NOG mice, mainly focusing on the differentiation and functions of the human B and T cells upon reconstitution.

Methods

$CD34^+$ hematopoietic stem cells

The cord blood from full-term deliveries was obtained from the Miyagi Cord Blood Bank, following the institutional guidelines approved by the Tohoku University Committee on Clinical Investigations. Some $CD34^+$ cell samples were obtained from the RIKEN Bioresource Center Cell Bank (Tsukuba, Japan). Mononuclear cells were isolated from cord blood by density gradient centrifugation using Lymphocyte Separation Medium (MP Biomedicals, Solon, OH, USA) after removing the phagocytes with Silica (Immuno Biological Laboratories, Takasaki, Japan). The cells were washed and suspended in PBS containing 5% FCS. $CD34^+$ stem cells were obtained by magnetic cell sorting (MACS) (Miltenyi Biotech, Bergisch Gladbach, Germany). Briefly, $CD34^+$ cells were labeled with a biotin-conjugated anti-human CD34 mAb (Serotec, Oxford, UK) after FcR blocking and subsequently with anti-biotin microbeads. The magnetically labeled $CD34^+$ cells were purified twice on LS columns. The usual purity of the $CD34^+$ fraction was >95%. The purified $CD34^+$ cells were cryopreserved in Cell Banker (Juji Field, Tokyo, Japan) at −80°C in a deep freezer until use.

Mice and reconstitution with human stem cells

Six-week-old female NOD/shi-scid/γc^{null} (NOG) mice were obtained from the Central Institute for Experimental Animals (CIEA) and maintained in the animal facility of Tohoku University School of Medicine under specific pathogen-free conditions. NOG I-$A\beta^{-/-}$ mice or NOG I-$A\beta^{+/-}$ mice were obtained by backcrossing B6 I-$A\beta^{-/-}$ mice (26) kindly gifted from Mathis and Benoist (Harvard Medical School) onto the NOG background more than five times with a speed congenic technique (27) in CIEA. All the animal experiments were properly conducted according to the institutional guidelines. These mice were irradiated with 120 cGy of X-rays, and 1×10^5 cord blood $CD34^+$ cells, which were resuspended with 200 μl PBS, were transferred into them by intravenous (i.v.) injection later the same day.

Antibodies and flow cytometric analysis

The following mAbs were used. Anti-CD3–FITC, anti-CD4–FITC, anti-CD19–FITC, anti-CD34–FITC, anti-CD45–FITC, anti-CD62L–FITC, anti-CD69–FITC, anti-CD4–phycoerythrin (PE), anti-CD20–PE, anti-CD23–PE, anti-CD44–PE, anti-IgD–PE, anti-CD4–allophycocyanin (APC), anti-CD20–APC, anti-CD28–APC, anti-CD38–APC, ani-IgM–APC, anti-CD11b–APC, anti-CD8–PE–Cy7, anti-CD3–biotin, anti-IgD–biotin and anti-CD132–biotin were purchased from BD PharMingen (San Jose, CA, USA). Anti-CD24–FITC, anti-CD27–PE, anti-CD23–PE, anti-CD10–PE, anti-CD178–PE, anti-CD95–pacific blue, anti-CD19–APC Alexa Fluor 750 and e-Fluor 450 Mouse IgG1, k isotype control were from e-Bioscience (San Diego, CA, USA). Anti-CD5–PE-Cy7 and anti-CD24–PE-Cy5 were from Beckman Coulter (Miami, FL, USA). Anti-CD34–biotin was from Serotec. Anti-TRBV28 (Vβ3)–biotin was from Ancell (Bayport, MN, USA). Biotinylated antibodies were visualized by streptavidin–APC or streptavidin–PE-Cy7 (BD PharMingen). For intracellular staining, anti-human IgM–FITC was purchased from Dako (Glostrup, Denmark). PE-labeled anti-VpreB (HSL96) and $V_{\lambda 5}$ (HSL11) were kindly provided by Karasuyama (28).

To analyze human lymphocytes in the hu-HSC-NOG mice, multicolor cytometric analysis was performed using a FACS

Calibur or FACS Canto II (BD Biosciences). To monitor the reconstitution periodically, peripheral blood was taken from the retro-orbital venous plexus through heparinized pipettes. At the time of sacrifice, single-cell suspensions were prepared from the spleen or BM by mincing with metal mesh or by flushing the tibiae and femurs with PBS containing 2% FCS using a 27-gauge needle. The cells were stained with the relevant mAbs for 15 min on ice, then washed with cold PBS containing 2% FCS and stained with the appropriate secondary antibodies when necessary. We used Cytofix/Cytoperm solution (BD Biosciences) for intracellular staining, according to the manufacturer's instructions. After the final wash, the cells were subjected to flow cytometric analysis. The proportion of each lineage was calculated using CELL Quest or FACS Diva software (BD Biosciences).

ELISA

The concentration of human IgM and IgG in the sera of reconstituted NOG mice was measured using a human Ig assay kit (Bethyl, Denver, CO, USA). For the detection of keyhole limpet hemocyanin (KLH)-specific human IgM and IgG antibodies, humanized NOG mice were immunized two or three times once a week with an emulsion of 500 μg of KLH whole protein (Sigma, St Louis, MO, USA) with CFA (Difco Laboratories, Sparks, MD, USA) in total 100 μl by intra-peritoneal (i.p.) injection. The sera from the immunized mice were harvested 1 week after the final immunization. The specific antibodies against KLH were measured by a standard ELISA. Briefly, 96-well plates were coated with 10 μg ml^{-1} KLH at 4°C overnight. After washing and blocking with PBS containing 1% BSA, the collected serum samples were loaded. HRP-conjugated anti-human Ig antibody was used as a secondary antibody. Both anti-IgG-specific and anti-IgM-specific antibodies were purchased from Bethyl (Montgomery, TX, USA). *o*-Phenylenediamine was used as a substrate for detection. The absorbance at 450 nm was measured by a microplate reader. To detect peptide-specific Ig, we used a peptide-coating kit (Takara, Otsu, Japan), according to the instruction manual.

To detect cytokines in the supernatants, kits for IL-2, IFN-γ or IL-4 (BD Biosciences) were used according to the instruction manuals from the manufacturer.

In vitro cultures

The single-cell suspension of spleen cells from hu-HSC-NOG mice was prepared as described above 16–20 weeks after reconstitution. Human IgD^+ mature B cells were isolated by MACS LS column by using a biotin-conjugated anti-IgD mAb and anti-biotin microbeads. The purity of the isolated fraction was ~90%. The IgD^+ cells were cultured in RPMI medium supplemented with 10% FCS and antibiotics [penicillin G sodium (100 U ml^{-1}) and streptomycin sulfate (100 μg ml^{-1})]. The cells were stimulated with polyclonal anti-IgM antibody at 2 μg ml^{-1} (Jackson Immunoresearch, West Grove, PA. USA) or with *Staphylococcus aureus* cowan (SAC) at 0.01% (Calbiochem, Gibbstown, NJ, USA) in the presence or absence of 1 μg ml^{-1} anti-CD40 antibody (R&D, Minneapolis, MN, USA) with or without a mixture of 100 ng ml^{-1} IL-21 (Peprotech, Rocky Hill, NJ, USA) and 25 U ml^{-1} IL-2 (R&D) in a 96-well plate (2×10^5 in 200 μl per well) for 7 days. The IgM and IgG levels in the culture supernatants were determined by ELISA as described above.

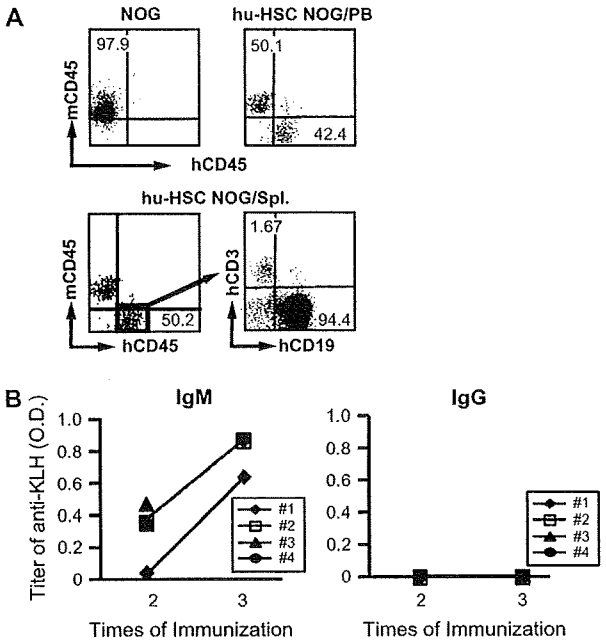

Fig. 1. Reconstitution of NOG mice with human hematopoietic stem cells. (A) Representative FACS analysis of peripheral blood (PB) cells from hu-HSC NOG mice 8 weeks after $CD34^+$ cell transplantation ($n = 6$). Engraftment of human $CD45^+$ ($hCD45^+$) cells in the PB in the hu-HSC NOG is shown (top left panel: control non-transferred NOG mouse, top right panel: hu-HSC NOG). Development of the human $CD19^+$ B cells and $CD3^+$ T cells in the spleen were analyzed in the hu-HSC NOG gated on $hCD45^+$ cells (bottom panels) (8 weeks after reconstitution, $n = 6$). (B) Humoral immune responses in hu-HSC NOG mice. Upon immunization of the hu-HSC NOG mice (at 16weeks after reconstitution, $n = 4$) with KLH/CFA emulsion (500 μg of KLH/CFA, three times), the sera was collected and examined for the presence of KLH-specific human IgM (left panel) or IgG (right panel) by ELISA.

For T-cell stimulation, the total spleen cells of hu-HSC NOG mice were cultured with PHA (1 μg ml^{-1}) or a mixture of soluble anti-CD3 (OKT3, 10 μg ml^{-1}) (BD PharMingen) and anti-CD28 (1 μg ml^{-1}) (Biolegend, San Diego, CA, USA) antibodies in a 96-well round-bottom plate (1×10^5 in 200 μl per well). Human $CD4^+$ or $CD8^+$ T cells in the hu-HSC NOG mice were purified by positive selection by MACS LS column in combination with anti-human CD4 or CD8 microbeads, respectively. The T cells were stimulated with immobilized anti-CD3 (10 μg ml^{-1}) and CD28 (1 μg ml^{-1}) antibodies or mixture of phorbol myristate acetate (50 ng ml^{-1}) and ionomycin (1 μg ml^{-1}) in 96-well round-bottom plates (1×10^5 in 200 μl per well). The T-cell proliferation was measured as the incorporation of [^{3}H]thymidine for the last 6 h of a 72-h culture. Carboxyfluorescein succinimidyl ester (CFSE) labeling was conducted according to a standard protocol.

Reverse transcription–PCR

The expression of mRNA for AID was measured by semi-quantitative reverse transcription (RT)–PCR. The total RNA

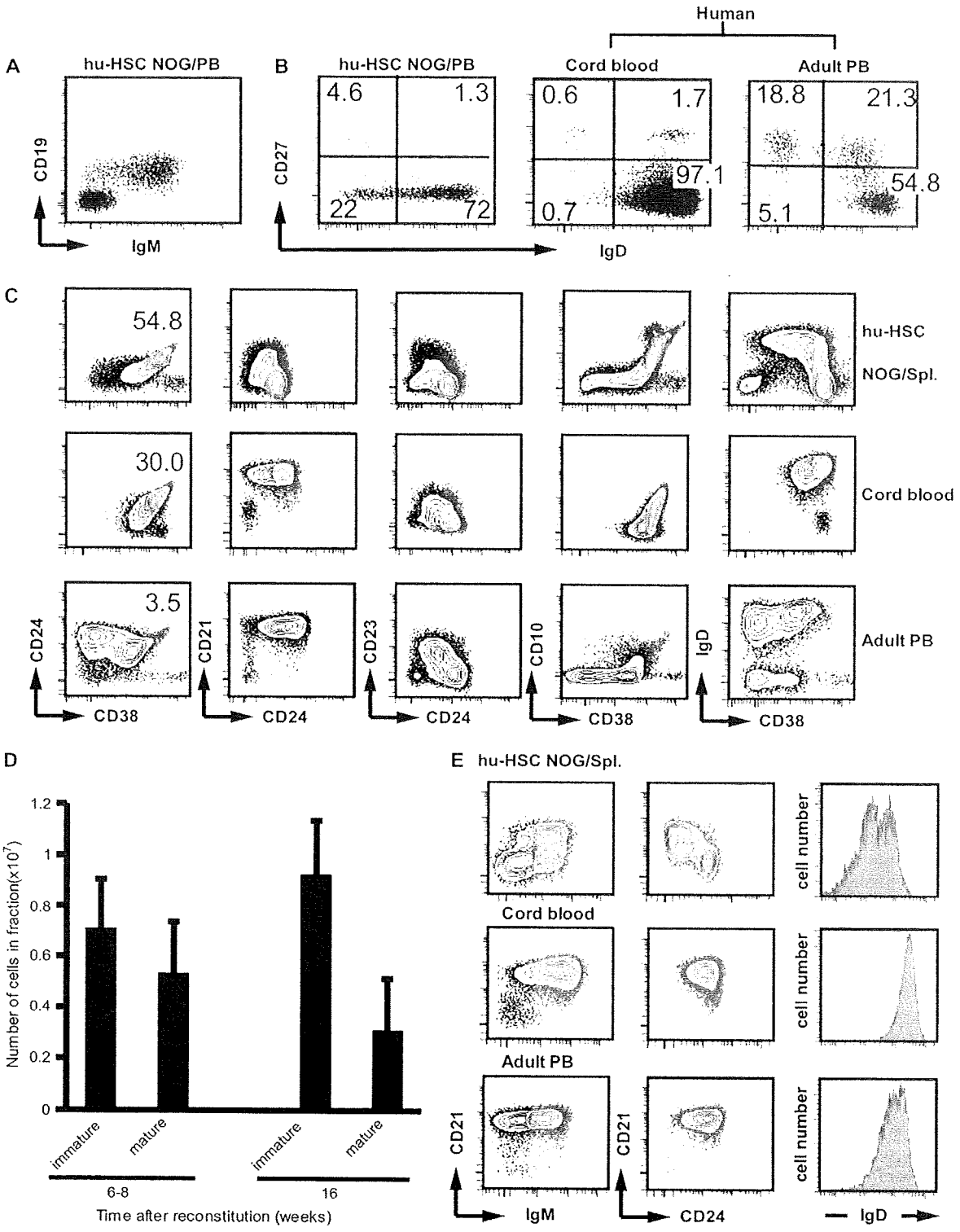

Fig. 2. Analysis of B cells in hu-HSC NOG. (A) Characterization of human B cells in the peripheral blood (PB) of hu-HSC NOG. A representative result of staining with anti-IgM and anti-CD19 antibodies was shown (16 weeks after reconstitution, $n = 6$). (B) Representative staining patterns with anti-IgD and anti-CD27 antibodies are shown gated on $CD19^+$ B cells from various sources [i.e. PB of the hu-HSC NOG (16 weeks after reconstitution, $n = 3$), human cord blood or PB of a normal healthy adult]. (C) A representative analysis of splenic $CD19^+$ cells in hu-HSC NOG by various differentiation-related markers. The whole-spleen cells of the hu-HSC NOG mice (8 weeks after reconstitution, $n = 4$), cord blood-derived

was prepared from cells using Trizol Reagent (Invitrogen, Carlsbad, CA, USA). The concentration of the total RNA was measured by NanoDrop 1000 (Nanodrop Technologies), and the first-strand cDNA was synthesized using SuperscriptIII (Invitrogen) with an oligo (dT) 20 primer. The cDNA for AID, RAG1, RAG2, TdT or glyceraldehyde 3-phosphate dehydrogenase (GAPDH) was amplified with specific primers using Ex-Taq polymerase (Takara). The primer sets were as follows—AID: forward, 5′-gaggcaagaagacactctgg and reverse, 5′-caaaaggatgcgccgaagctgtctggag; RAG1: forward, 5′-ccagctgtttgcttggccatccgt and reverse, 5′-ttgggatctcatgccttccaagat; RAG2: forward, 5′-atgtccctgcagatggtaaca and reverse, 5′-gcctttgtatgagcaagtagc; TdT: forward, 5′-ccaccaattgctgtacaaaaga and reverse, 5′-tcgttcatcatttaacacagctt; β-actin: forward, 5′-gctcgtcgtcgacaacggctc and reverse, 5′-caaacatgatctgggtcatcttctc and GAPDH: forward, 5′-gaaggtgaaggtcggagtca and reverse, 5′-ttcacacccatgacgaacat.

After denaturing at 94°C for 5 min, the cDNA was amplified by a protocol consisting of 94°C for 30 s, 60°C for 30 s and 72°C for 30 s, for 25 cycles. The PCR products were separated on agarose gels and stained with ethidium bromide.

Retroviral vectors

The retroviral vector, pDΔNsam-IRES-EGFP, based on murine stem cell virus with enhanced green fluorescent protein (EGFP) as a marker under an internal ribosomal entry site (IRES) was kindly provided by Onodera (29). PLAT-F, a package cell line that produces a pseudotype virus with an RD114 envelope, was from Kitamura (30) and used to infect $CD34^+$ stem cells. The human *bcl-2* or *HLA-DRB*0401* genes were inserted into the *Not*I and *Bam*HI sites of the pDΔNsam-IRES-EGFP vector.

B16 T cells specific for an influenza hemagglutinin peptide ($HA_{307-319}$) were kindly provided by Buckner (31). The T-cell receptor (TCR) genes (B16 TCR; *TRAV4* and *TRBV28* based on the International Immunogenetics Information System) were isolated by standard techniques from the B16 T cells and cloned into the retroviral vector. *TRAV4* was inserted into the *Not*I/*Bam*HI sites, while *TRBV28* was inserted into the *Nco*I/*Cla*I sites after removing the EGFP gene. To infect human T cells, retrovirus was prepared in the form of a VSV-pseudotype virus in 293T packaging cells, by plasmid DNA transfection using a standard calcium phosphate protocol. After 72 h, the supernatants were recovered and concentrated by centrifugation at 8700 r.p.m. for 19 h at 4°C.

Gene delivery into $CD34^+$ cells by retrovirus

$CD34^+$ cells isolated from cord blood were cultured in X-VIVO 15 (Cambrex Bioscience, Walkersville, MD, USA), supplemented with 1% human serum albumin (HSA) (Kaketsuken, Kumamoto, Japan) and stimulated with a cytokine cocktail [100 ng ml^{-1} stem cell factor (R&D), 100 ng ml^{-1} Flt-3 ligand (Flt-3L) (R&D), 100 ng ml^{-1} thrombopoietin and 100 ng ml^{-1} IL-6 (Peprotech)] in a 24-well plate (2×10^5 per well) for 48 h. During the priming of the $CD34^+$ cells, non-tissue culture-treated six-well plates (Becton Dickinson) were coated with CH-296 recombinant fibronectin fragment (Retronectin) (20 μg ml^{-1}, Takara). The stimulated $CD34^+$ cells were harvested and placed in the CH-296-coated plates (3×10^5 per well) in the presence of the respective virus supernatant. The supernatants were diluted 1:2 with X-VIVO containing 1% HSA, 10 μg ml^{-1} protamine sulfate and the cytokine mixture described above. The cells were spun at 2000 r.p.m. for 30 min at 37°C. Every 12 h, the medium was replaced with fresh virus supernatant. After 48 h of culture, the frequency of GFP- and CD34-expressing cells was examined. About 5×10^5 to 1×10^6 infected cells were injected i.v. into irradiated NOG mice.

Retroviral infection of human T cells

$CD4^+$ T cells were isolated from the PBMCs of normal healthy donors by MACS, as described above. The infection of T cells by retrovirus for B16 TCR was conducted as previously reported (32). Briefly, purified T cells were stimulated in the presence of recombinant human IL-2 (50 U ml^{-1}) on a 24-well plate that had been previously coated with anti-CD3 antibody (1 μg ml^{-1}), anti-CD28 antibody (1 μg ml^{-1}) and Retronectin (12 μg ml^{-1}). Half of the culture medium was replaced by fresh medium supplemented with IL-2 every 48 h. On days 4 and 5, the T cells were spin-infected with the concentrated virus (2000 r.p.m., 90 min at 32°C). After a further 1 week of culture, the expression of B16 TCR on the T cells was examined by staining with anti-TRBV28 antibody, APC-conjugated HLA-DRB1*0401/$HA_{307-319}$ (PKYVKQNTLKLAT) or HLA-DRB1*0401/human $CLIP_{103-117}$ (PVSKMRMATPLLMQA) tetramers (kindly provided by National Institute of Health tetramer core facility). These T cells (1×10^6 or 3×10^6) were transferred into reconstituted NOG mice by i.v. injection and subsequently i.p. immunized with HA peptide/CFA emulsion (100 μg HA peptide in total 100 μl).

Results

Reconstitution of NOG mice with human $CD34^+$ stem cells

In the fully reconstituted NOG mice, a significant amount of human B and T cells appeared in the peripheral blood and comprised major fractions in the spleen, as previously reported (16) (Fig. 1A). Immunization of the hu-HSC NOG mice with a protein antigen, KLH, with CFA evoked an antigen-specific IgM response, but a negligible antigen-specific IgG response (Fig. 1B). This finding was also consistent with previous reports (21, 22, 24, 25).

Analysis of the human B cells in hu-HSC NOG mice: partial differentiation of the human B cells

To elucidate the mechanisms for the poor IgG response in the hu-HSC NOG mice, we analyzed the development and

cells or PB from a normal adult were stained with respective antibodies. $CD24^{int/hi}CD38^{hi}$ immature population is highlighted by red contour plot. (D) The number of immature ($CD19^+CD24^{int/hi}CD38^{hi}$) or mature ($CD19^+CD24^{lo}CD38^{lo}$) B cells from hu-HSC NOG at different time points after reconstitution. The means of the cell number of each B-cell population are represented with standard deviation ($n = 3$ for each group). (E) Partial differentiation of human B cells in the spleen in hu-HSC NOG mice. The expression patterns of CD24, CD21 or IgD on $CD19^+IgM^+$ B cells (highlighted by blue contour plot) from the hu-HSC NOG mice (8 weeks after reconstitution, $n = 4$), cord blood or adult PB are shown.

differentiation of the human B cells in these mice in detail. Most of the human B cells in the peripheral blood of the hu-HSC NOG mice were IgM and/or IgD positive (Fig. 2A). Few $CD27^+$ B cells were detected, indicating that almost all the B cells were in a naive state (Fig. 2B). This phenotype was different from that of the human B cells in PBMCs obtained from normal healthy donors or cord blood, which clearly consisted of three major subsets: $IgM^+IgD^+CD27^-$-naive B cells, $IgM^+IgD^+CD27^+$-activated or non-switched memory B cells and IgD^-CD27^+ memory B cells (Fig. 2B).

The analysis of the human B cells in the spleen from the hu-HSC NOG mice for two developmentally regulated markers, CD24 and CD38, revealed an unusual accumulation of $CD24^{int/hi}CD38^{hi}$ immature B cells in the spleen (Fig. 2C). This $CD24^{int/hi}CD38^{hi}$ population comprised up to 60% (62.0 ± 13.8%, $n = 6$) of the splenic $CD19^+$ cells on average in the hu-HSC NOG mice. The frequency was lower at early time points after reconstitution but gradually increased; i.e. ~50% (53.3 ± 8.0%, $n = 3$) 6–8 weeks after reconstitution and ~70% (70.7 ± 13.7%, $n = 3$) 16 weeks after (Fig. 2D). Although a similar $CD24^{int/hi}CD38^{hi}$ population was also evident in the cord blood B cells or PBMCs (~30% or 2–3% in $CD19^+$ cells, respectively) (Fig. 2C), the $CD24^{int/hi}CD38^{hi}$ population in the hu-HSC NOG mice showed an even more immature phenotype (Fig. 2C); i.e. the former was $CD21^{hi}$ $CD23^{int}CD10^{lo}$ IgD^{hi}, while the latter was $CD21^-CD23^-CD10^{int/hi}IgD^{-/lo}$. Besides the $CD24^{int/hi}CD38^{hi}$ population, even when gated on more mature IgM^+ B cells, ~25% of the cells in the hu-HSC NOG mice were still $CD24^{hi}CD21^-IgD^{-/lo}$ (Fig. 2E), resembling the phenotype of transitional type 1 (T1) B cells (33). These analyses collectively suggested that the human B cells were only partially differentiated in the hu-HSC NOG mice.

Accumulation of B-cell precursors in the spleen of hu-HSC NOG mice

We also noticed the presence of a large number of $CD19^+CD24^{int/hi}CD38^{hi}IgM^-IgD^-$ cells (~40% of the $CD19^+$ population) in the spleen of the hu-HSC NOG mice (Fig. 3A, left panel). Because of their immature phenotype, we suspected these cells to be B-cell progenitors. Further dissection of the $CD19^+IgM^-IgD^-$ population using anti-CD20 and CD34 antibodies demonstrated that they consisted of at least three fractions: $CD20^-CD34^+$, $CD20^-CD34^-$ and $CD20^+CD34^-$ B cells (Fig. 3A, right panel). Since B cells with these phenotypes are known to comprise immature B-cell lineages in the BM, we examined the BM cells in the hu-HSC NOG mice. As expected, $CD19^+IgM^-CD20^-CD34^+$ pro-B and $CD19^+IgM^-CD20^-CD34^-$ pre-B cells were detected (Fig. 3B). The expression of CD179 (V_{preB}) and cytoplasmic μ chain (cμ) was also examined by intracellular staining. There were three distinct populations with different expression patterns for CD179 and cμ: $CD179^+c\mu^-$ pro-B, $CD179^+c\mu^+$ pre-B and $CD179^-c\mu^+$ populations, both in the spleen and BM (Fig. 3C and D). We obtained similar results for $V_{\lambda 5}$ (data not shown). RT–PCR analyses showed that the pro-B- or pre-B-like cells in the spleen expressed RAG and TdT, with patterns similar to those of the pro-B and pre-B cells in the BM (Fig. 3E).

In addition to the presence of phenotypically pro-B- and pre-B-like cells in the spleen of the hu-HSC NOG mice, further immature B-cell lineages, i.e. early-B cells or common lymphoid progenitors, were detected in the spleen. Using CD38 and CD10 (34, 35), a clear $CD19^-CD38^+CD10^+CD34^+$ early-B-cell population was detected in the spleen as well as in the BM (Fig. 3F and G). These results collectively suggest that early precursors in the B-cell lineage were present in the spleen of the humanized NOG mice.

IgG response of the human B cells from hu-HSC NOG mice to in vitro stimulation

The poor production of IgG in the hu-HSC NOG mice might have been attributed to the inappropriate differentiation of human B cells in the mouse environment. To examine the intrinsic capability of the B cells for the IgG response, we used an *in vitro* culture system. IgD^+CD19^+-naive mature B cells were purified from the spleen of hu-HSC NOG mice and stimulated with SAC as quasi-antigens in the presence or absence of anti-CD40 antibody. IL-21/IL-2 was also provided because these cytokines, especially IL-21, are potent inducers of naive B-cell differentiation into antibody-secreting cells *in vitro* (36, 37). Significant amounts of both IgM and IgG were detected in the supernatants after a 7-day culture (Fig. 4A). The IgG level was comparable to that of normal B cells from healthy donors (data not shown). Antigenic stimulation together with IL2/IL-21 also induced the formation of IgD^-CD38^+ antibody-secreting cells (Fig. 4B). In addition, IgD^-CD27^+ cells appeared toward the end of the culture period (Fig. 4B). The antibody class switch in these B cells was further supported by the induction of AID mRNA in the cultured B cells (Fig. 4C). These results suggested that the human B cells with a mature phenotype in hu-HSC NOG mice could respond to antigenic stimulation and had the functional molecular machinery for the Ig class switch.

Analysis of the human T cells in hu-HSC NOG mice: impaired function of $CD4^+$ T cells

Since the human B cells from hu-HSC NOG mice could produce IgG *in vitro*, we next examined the T cells in the hu-HSC NOG mice. The development of human $CD4^+$ and $CD8^+$ T cells was detected in the thymus and spleen of the hu-HSC NOG mice (Fig. 5A). Initially, we compared the expression patterns of several T-cell-related antigens and cytokine receptors: CD28, CD44, CD62L, CD132 (γc) and IL-7Rα chain (Fig. 5B). There were, however, no significant differences in these molecules between the T cells from the hu-HSC NOG mice and PBMCs.

To address the functionality of the T cells, we stimulated the whole-spleen cells from hu-HSC NOG mice with PHA or a mixture of soluble anti-CD3 and anti-CD28 antibodies in *in vitro* culture systems. The hu-HSC NOG spleen cells showed significant proliferation after 3 days in culture, consistent with previous reports (Fig. 5C). However, when the whole-spleen cells from the hu-HSC NOG mice previously immunized with KLH were re-stimulated in the presence of KLH *in vitro*, we could hardly detect IFN-γ and IL-4 (data not shown). This result was in agreement with the poor IgG production in the hu-HSC NOG mice.

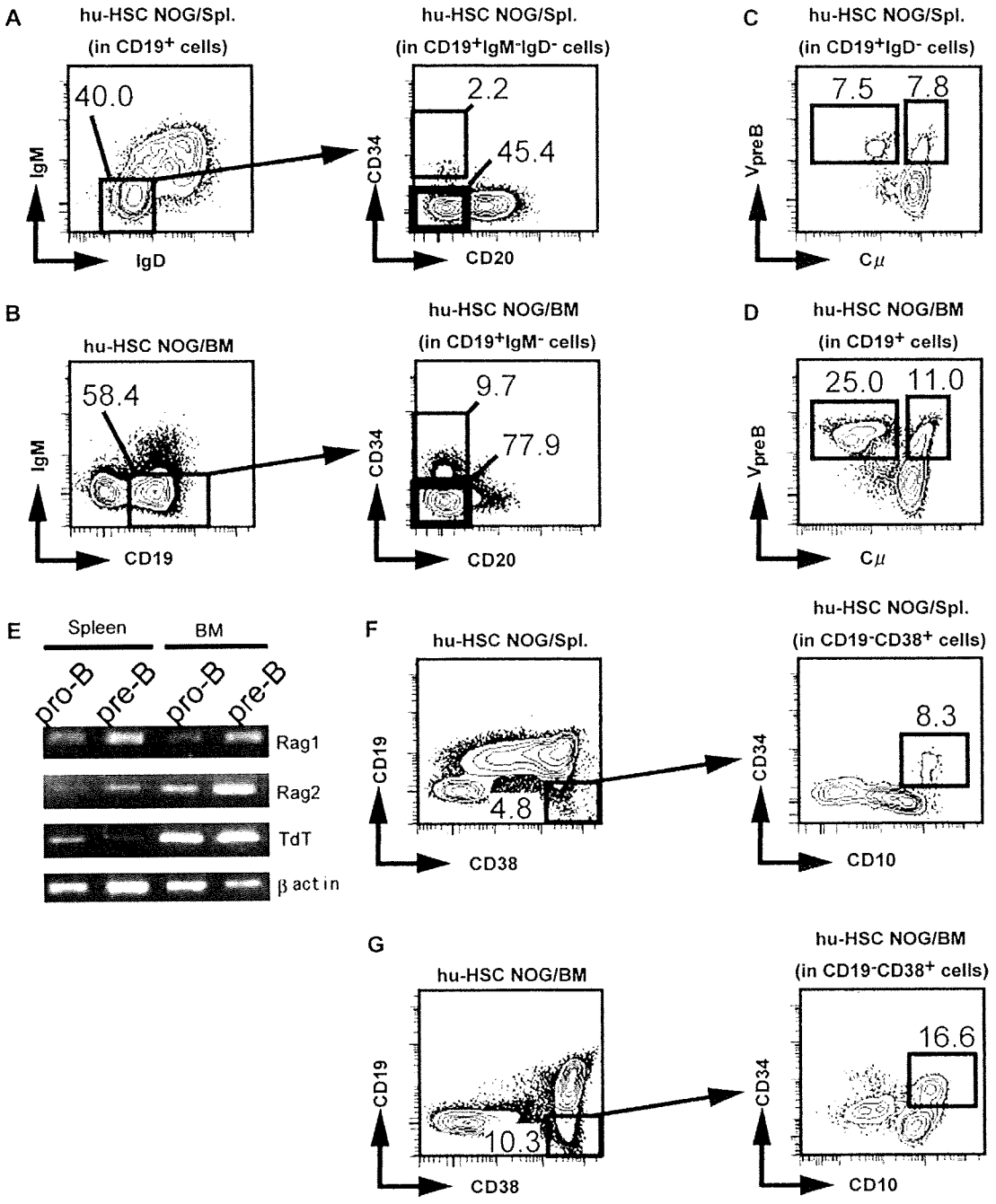

Fig. 3. Accumulation of human B-cell progenitors in the spleen of hu-HSC NOG mice. (A and B) Representative staining data of spleen (A) or BM (B) of hu-HSC NOG mice. The spleen cells or BM from hu-HSC NOG mice (8 weeks after reconstitution, $n = 4$) were stained with anti-CD19, anti-IgM and anti-IgD antibodies as described in Methods (left panels). The $CD19^+IgD^-$ IgM^- or $CD19^+IgM^-$ cells (represented by rectangles) in the spleen or BM, respectively, were further analyzed for the expression of CD34 and CD20. $CD34^+CD20^-$ (gated by thin rectangle) or $CD34^-CD20^-$ B cells (gated by bold rectangle) represent pro-B or pre-B cells, respectively. (C and D) Expression of V_{preB} in B cells in hu-HSC NOG mice. $CD19^+IgD^-$ cells in the spleen (C) or $CD19^+$ cells in BM (D) were examined for V_{preB} with cμ by intracellular staining (8 weeks after reconstitution, $n = 3$). The gated $V_{preB}^+c\mu^-$ or $V_{preB}^+c\mu^+$ cells represent pro-B cells or pre-B cells, respectively. (E) Analyses of gene expression in human B-cell progenitors in hu-HSC NOG mice. cDNA was prepared from $CD19^+IgM^-$ $CD34^-$ $CD10^+$ pre-B or $CD19^+IgM^-$ $CD34^+CD10^+$ pro-B cells in the spleen or BM of the hu-HSC NOG mice (8 weeks after reconstitution). The expression of RAG-1, RAG-2 or TdT was examined by semi-quantitative RT–PCR as described in Methods. A representative result of three independent experiments is shown. (F and G) Detection of early-B cells in the spleen (F) or BM (G) in hu-HSC NOG mice. Cells were stained with anti-CD19 and anti-CD38 antibodies (left panels). The expression of CD10 and CD34 in $CD19^-$ $CD38^+$ gated cells were further examined (8 weeks after reconstitution, $n = 3$). The gated $CD19^-$ $CD38^+CD10^+CD34^+$ cells represent early-B or common lymphoid progenitors cells.

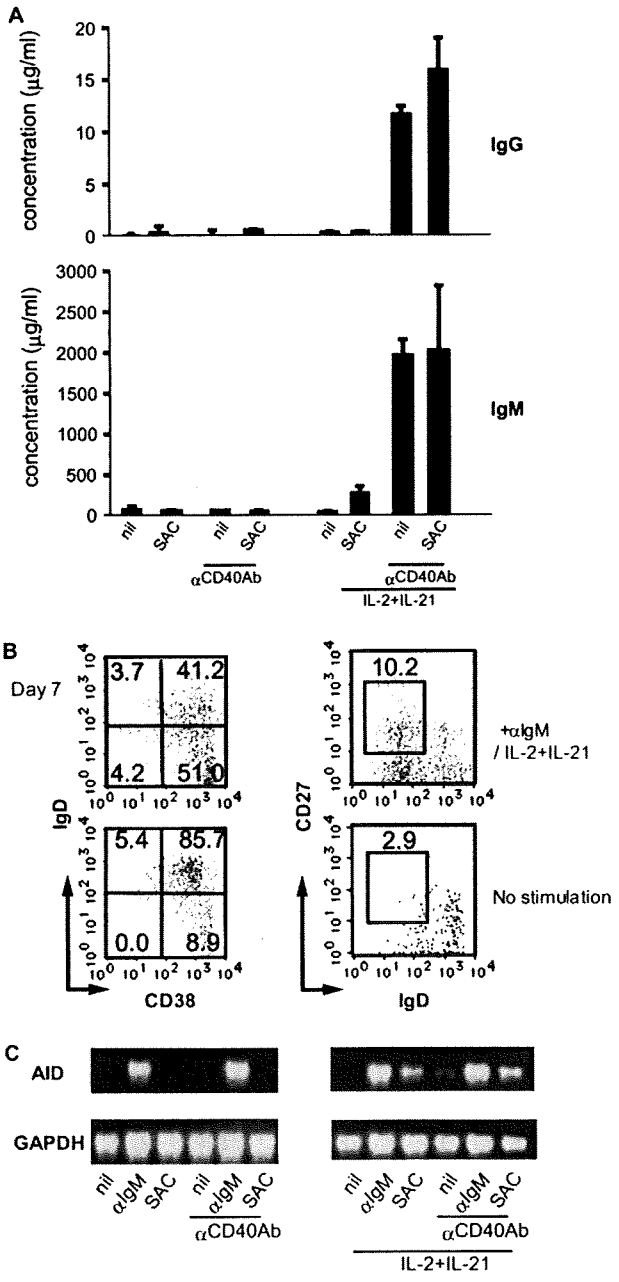

Fig. 4. Analysis of immune response of human B cells in hu-HSC NOG mice *in vitro*. (A) Purified IgD$^+$ splenic B cells in the hu-HSC NOG mice (8–16 weeks after reconstitution, $n = 4$) were stimulated *in vitro* with SAC (0.01%), in the presence or absence of anti-CD40 polyclonal antibody (1 μg ml^{-1}), with or without IL-2 (25 U ml^{-1})/IL-21 (100 ng ml^{-1}); secretion of IgM and IgG by 7-day cultured human B cells. Each culture supernatant was harvested and the amounts of human IgM (lower panal) and IgG (upper panel) were quantified by ELISA as described in Methods. (B) Analysis of surface antigen expression on CD19$^+$ splenic B cells in hu-HSC NOG mice (8–16 weeks after reconstitution) after *in vitro* stimulation with or without polyclonal anti-IgM antibody and cytokines. After 1-week culture, the B cells were recovered and stained with anti-CD38, anti-CD27 and anti-IgD antibodies. A representative result of three independent cultures is shown. (C) Total RNA was extracted from the B cells 3 days after *in vitro* culture with various stimulations, followed by synthesis of cDNA. The expression of AID or GAPDH was investigated by RT–PCR. A representative result of three independent cultures is shown.

Although we observed the activation of the spleen cells of the hu-HSC NOG mice, the magnitude was quite low compared with that of the cultured PBMCs. To exclude the contributions of antigen-presenting cells and analyze the T cells directly, we used purified CD4$^+$ and CD8$^+$ T cells. When the purified T cells were stimulated with immobilized anti-CD3 and anti-CD28 antibodies, they showed significant proliferation compared with the culture without stimulation. However, the intensity of their response, especially that of the CD4$^+$ T cells, was markedly lower than that of normal T cells isolated from PBMCs (Fig. 6A, left panel). The cumulative data showed that the magnitude of the proliferation of CD4$^+$ T cells from the hu-HSC NOG mice was no more than 10% of the normal CD4$^+$ T-cell response (Fig. 6A, right panel). For the CD8$^+$ T cells, the tendency was less clear because there was a large variance among mice (Fig. 6A). The T cells from the hu-HSC NOG mice also showed only modest proliferation even when they were strongly stimulated with PMA and ionomycin (Fig. 6B). The amount of IL-2 produced by the cultured T cells was remarkably low, consistent with their low proliferation (Fig. 6C). Addition of exogenous IL-2 (100 IU ml^{-1}) did not restore the proliferation of the human T cells from the hu-HSC NOG mice (data not shown).

Mechanisms of the impaired response of the human T cells in hu-HSC NOG mice

To examine the mechanisms of the hyporesponse of the T cells in the hu-HSC NOG mice, we analyzed the expression of CD25 and CD69 after stimulation. These molecules were detected on both CD4$^+$ and CD8$^+$ T cells, at similar levels as on normal T cells from PBMCs (Fig. 7A). When the number of viable cells was enumerated, however, there were significant differences between the hu-HSC NOG T cells and PBMC T cells. AnnexinV and propidium iodide (PI) staining of cultured T cells demonstrated that >50% of the CD4$^+$ T cells from hu-HSC NOG mice were dead at 24 h, while only 10% of the PBMC T cells were (Fig. 7B). At 48 h, nearly 80% of the CD4$^+$ T cells from hu-HSC NOG mice were PI positive. The CD8$^+$ T cells showed different patterns among mice. In the half of the animals, nearly 80% of the CD8$^+$ T cells died after a 24-h culture, while in the remaining half, 60% of the cells were still alive after a 72-h culture (Fig. 7C). To investigate the higher susceptibility of the T cells in the hu-HSC NOG mice to cell death, we examined the expression of CD95 (Fas) and CD178 (FasL) on the T cells. A significant expression of CD95 (Fig. 7D) but not CD178 (data not shown) was detected on the T cells from the hu-HSC NOG mice. In the human T cells from PBMCs, there were two populations, CD95$^+$ and CD95$^-$, while in the hu-HSC NOG mice, most of the T cells expressed similar amounts of CD95 on their surface (Fig. 7D).

We next addressed whether the impairment of T-cell functions was already conferred to the T cells in the thymus of the hu-HSC NOG mice. CD4$^+$CD8$^-$ single-positive (SP) thymocytes were prepared from the hu-HSC NOG mice. Because the number of thymocytes in a hu-HSC NOG mouse was usually not sufficient for analysis, we introduced the *bcl-2* gene into the CD34$^+$ stem cells by retrovirus *in vitro* before transplantation in an effort to increase the cell number. Indeed, in such hu-HSC (*bcl-2*) NOG mice, the

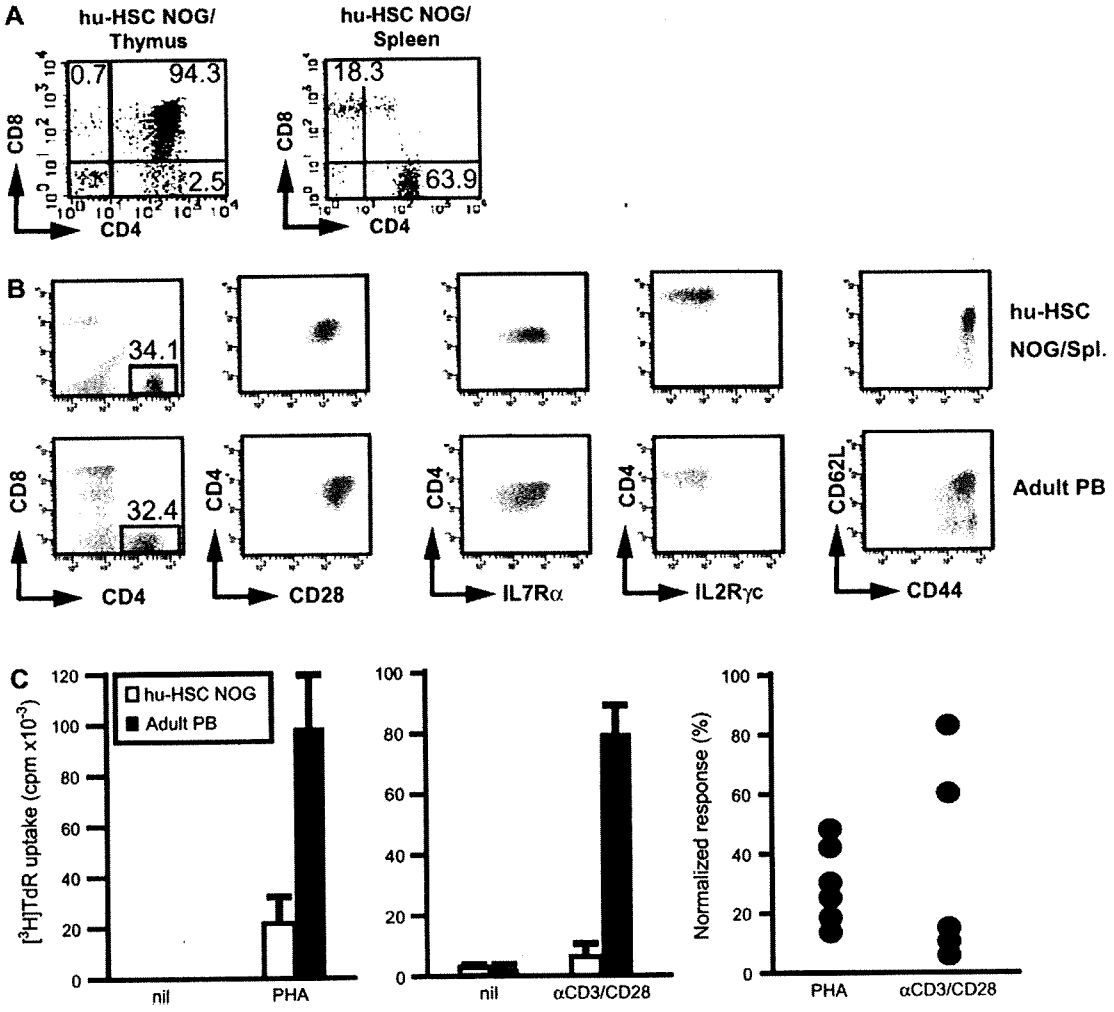

Fig. 5. Analysis of human T cells developed in hu-HSC NOG mice. (A) Development of human T cells in the thymus and spleen in hu-HSC NOG mice. Single-cell suspensions from each organ were stained with anti-CD4 and anti-CD8 antibodies (20 weeks after reconstitution, $n = 4$). (B) A representative staining for various molecules on human T cells from hu-HSC NOG mice. Whole-spleen cells from the hu-HSC NOG mice (20 weeks after reconstitution, $n = 3$) or adult peripheral blood (PB) were stained with indicated antibodies. $CD4^+$ T-cell population (gated by rectangles and highlighted by red dot plots) was further examined for each molecule. (C) Analysis of functions of human T cells in hu-HSC NOG mice *in vitro*. Whole splenocytes from the hu-HSC NOG mice (20 weeks after reconstitution) (white bar) or normal adult PB (black bar) were stimulated with PHA (left panel, $n = 6$) or mixture of soluble anti-CD3 and anti-CD28 antibodies (middle panel, $n = 5$). After 72-h culture, the proliferation of T cells was measured as the amounts of incorporated [^{3}H]thymidine ([^{3}H]TdR). Representative data are shown. The means from triplicated cultures are shown. The cumulative data are shown after normalizing the magnitude of the response of hu-HSC NOG T cells to that of PB T cells (right panel).

exogenous Bcl-2 was expressed at a high level (Fig. 8A), and the effect on increasing the thymocytes was remarkable (no more than 1×10^6 in each mouse with control GFP vector versus $\sim 6 \times 10^6$ in *bcl-2* group), although the differentiation of B or T cells in the spleen was not affected (data not shown). We isolated the $CD4^+CD8^-$ SP thymocytes or splenic $CD4^+$ T cells from the hu-HSC (*bcl-2*) NOG mice and stimulated them as described above. The $CD4^+CD8^-$ SP cells showed vigorous proliferation, as high as that of normal T cells from PBMCs (Fig. 8B). A significant amount of IL-2 was also detected in the culture supernatants of the $CD4^+CD8^-$ SP cells (Fig. 8C). Interestingly, the splenic $CD4^+$ T cells from the same mice did not show proliferation (Fig. 8B). Consistently, immunization of the hu-HSC (*bcl-2*) NOG mice did not evoke an immune response in spite of the improvement in cell number (data not shown). Thus, the unresponsiveness of the T cells in the hu-HSC NOG mice was induced in the periphery, not in the thymus. Notably, the $CD4^+$ T cells from the hu-HSC (*bcl-2*) NOG mice showed better viability compared with the $CD4^+$ T cells from the usual hu-HSC NOG mice; 60–80% of the cultured cells were still viable after 48 h (data not shown). Hence, the poor response of the T cells from hu-HSC NOG mice was not solely due to their high susceptibility to cell death, but other mechanisms (such as induction of anergy) were also involved.